Yurok Tribe
Fisheries Department

Stream bed disturbance and risk of salmonid redds scour in the Trinity River, CA

Technical Report
To the Trinity River Restoration Program

1313 S. Main St.
Weaverville, CA 96093

Prepared by:
David Gaeuman and Kyle De Juilio
Yurok Fisheries Department

and

Todd Buxton
Trinity River Restoration Program

February 2023

Contents

Abstract

Stream bed disturbance during high-flow events is a normal consequence of a natural hydrologic regime. Bed disturbance can be beneficial to some aquatic organisms and some life stages of individual species but can also pose risks to other organisms and/or life stages. Among the benefits to salmonids, bed disturbance can shift macroinvertebrate species composition and abundances from that of large, long-lived species to smaller, shorter-lived ones that are more available as prey for juvenile salmonids. High flow events during the salmonid egg incubation season, however, also have the potential to scour the stream bed to depths that cause mortality of salmonid eggs or alevins. This study investigates the extent and magnitude of stream bed disturbance generated by winter flood events in the Trinity River between Lewiston Dam and the North Fork Trinity River to assess the potential for generating beneficial bed disturbance that stimulates trophic production and other ecosystem services, as well as the potential risk that deep bed scour might pose to salmonid redds. We evaluate bed mobility with dimensionless shear stresses (τ^*) derived from modeled shear stresses and a map of estimated median bed surface grain sizes throughout the study area. Discharges considered range from flows that generate shear stresses near the threshold of coarse sediment entrainment in the river up to the maximum authorized flow release from Lewiston Dam coupled with spring 100-year tributary flood events. The full study area is divided into seven segments, each of which is defined by major tributary confluences and characterized by different hydrology. For each segment, the extent of the stream bed subject to beneficial bed disturbance at different discharge levels is quantified by the fraction of bed area where τ^* exceed 0.03. Likewise, the risk that salmonid redds could be scoured to the depth of their egg pockets is assessed in terms of the fraction of mapped salmonid redds located where τ^* exceed thresholds for significant bedload transport and full stream bed mobility (0.06). We find that the range of floods considered herein will disturb between 25% and 60% of the stream bed area, depending on stream segment, but that the risk of scouring salmonid redds is comparatively small. In most of the study area, redds tend to be at locations where shear stresses are larger than the average for the full stream bed at small discharges but increase relatively slowly or decrease as discharge increases. Redd locations are nearly twice as likely to exhibit shear stress reversals (decreasing shear stress with increasing discharge) than the general stream bed in six of the seven river segments. Only in segment 1, which includes a high concentration of redds in an artificial channel adjacent to the Lewiston Fish Hatchery, is the proportion of shear stress reversals at redd locations and over the full bed similar. Prior research in the Trinity River suggests that the probability of bed scour to depths sufficient to harm salmonid eggs is about 8% for τ^* greater than 0.06 and about 3% for τ^* between 0.04 and 0.06. Our results indicate that the maximum floods modeled will produce τ^* greater than 0.06 at between 5% and 23% of all redd locations, whereas 0.045 is exceeded at between 15% and 40% of redd locations. Combined with probabilities of deep scour reported in the literature, these areal percentages yield an estimated risk of scour to individual redds during a maximum flood over the full study area of about 2.3%.

Introduction

Background

Substrate in gravel-bed channels provides habitat for macroinvertebrate assemblages and salmonid nest ("redd") construction, egg incubation, and early rearing. During high flows, these habitats can be disrupted by mobilization of the bed surface and scour of the stream bed to depths where these species reside. Species have variable adaptations to disturbance which determine resiliency or recovery. The disturbance can shift macroinvertebrate species composition and abundances from that of large, long-lived species to smaller, shorter-lived ones that are more available as prey for salmonids (Wooton et al. 1996) or native species which are exploited by salmonids at a higher rate than non-native ones (Cross et al. 2011). This shift and associated boost in prey can benefit salmonids by increasing feeding opportunities and the consequent size of individuals and biomass of the population (Cross et al. 2011). It has been documented in the neighboring Eel River that the abundance and proliferation of *Dicosmoecus sp.* and other invulnerable prey species are tied to cycles of bed disturbance and vulnerability to scour (Power et al. 2008; Wooton et al. 1996). The same species assemblages exist on the Trinity River with even greater flow regulation and diversion. Bed mobility and scour also benefit salmonids by reducing numbers of the oligochaete worm *Haplotaxis ichthyophagous* that preys on salmonid eggs in stream beds. Bed mobilization can also flush biomatter and fine sediments from the stream bed and increase hyporheic flow through the bed, which can improve incubation conditions in redds (Sparkman, 2003). However, sediment mobility and scour can also negatively affect salmonid early life stages (Buxton et al., 2015; Tonina and Buffington, 2009) when scour reaches depths that endanger eggs or alevins by exposing them to flow and predation or death by mechanical crushing (Montgomery et al., 1996).

The relative timing of scour and egg incubation have a strong role in determining incubation success. Chinook and coho salmon spawning occurs in the Trinity River from September through January. The September start date is just prior to the wet season that generally lasts from November through May in the region. In this period, high flows are common in the historic record for the Trinity River and unregulated tributaries. In the regulated Trinity River, flow releases from Lewiston Dam are 450 cubic feet per second (ft^3/s) until October 15 and then 300 ft^3/s until around April 16 when peak flows up to 11000 ft^3/s are released in accordance with the Trinity River Record of Decision (USDOI, 2000). While high flows that scour the channel bed occasionally occur below major tributaries, flood frequency and magnitude in the incubation period are much lower than prior to the start of flow regulation in November 1960. Flood suppression by dam operations reduce risk to eggs in redds from scour, but high flow events on tributaries can increase river flows with distance from Lewiston Dam and pose a risk of scouring developing embryos and macroinvertebrate assemblages in the bed.

In addition to timing, bed disturbance effects on salmonid incubation are controlled by the magnitude of high flows, substrate caliber, redd location, and depth of egg burial in the stream bed. The latter is controlled by female body size, since bigger fish can move a larger range of sediment sizes to a greater depth because of their increased torque relative to shorter, smaller fish (Riebe et al., 2014). Concerning Chinook salmon (*Oncorhynchus tshawytscha*) redds in the portion of the Trinity River targeted for fisheries restoration (between Lewiston Dam and the North Fork Trinity River), Evenson (2001) measured egg pockets for 28 redds and found depths

ranged from 6 to 52 cm with a mean of 23 cm and 30 cm to the top and bottom of the egg pocket, respectively. Prior to the eyed stage of development, which lasts around a month after fertilization depending on temperature, eggs are most sensitive to disturbance (Murray and McPhail 1988). Thereafter, eyed eggs are substantially more hardy and less susceptible to mortality from bed movement, and salmonids in the alevin stage can escape areas of partial bed mobility by moving deeper in the bed via interstitial spaces between sediments (Bjornn and Reiser, 1991).

We estimate the probability of bed surface mobility and scour to egg pocket depths by flood discharges between 4000 and about 23200 ft^3/s in the Trinity River between Lewiston Dam and the North Fork Trinity River. For this, we use modelled basal shear stresses in the channel with estimates of bed surface grain size to compute dimensionless shear stresses. The resulting values are evaluated against an empirical relationship between dimensionless shear stress and potential for deep stream bed scour that May et al. (2009) developed for a reach of the Trinity River. We also compare estimated dimensionless shear stresses to critical values published in the literature for gravel-bed channels to identify areas where bed disturbance levels are sufficient to shift the composition and abundance of the macroinvertebrate community. We predict that redds are primarily constructed in areas of the channel that are not prone to deep scour. We further hypothesize that relatively widespread stream bed disturbance, which could seasonally shift macroinvertebrate community structure in the Trinity River to favor salmonids, can be accomplished by flow magnitudes that mobilize the stream bed while posing little risk to incubating salmonid eggs. Throughout the remainder of the manuscript stream bed disturbance or mobilization is referenced as a surrogate for the beneficial ecological services of coarse stream bed maintenance and shifts in the macroinvertebrate community that favor salmonid forage. Restoring the natural timing of stream bed disturbance could help promote seasonal food subsidies to salmonids. We evaluate tradeoffs of bed disturbance during salmonid incubation by examining the effects of a recent proposal to increase the occurrence and magnitude of winter floods caused by Lewiston Dam releases during high tributary flow events.

Study Area

The study area for this investigation is the section of the Trinity River identified for rehabilitation in the Trinity River Record of Decision (USDOI 2000), which established the Trinity River Restoration Program (TRRP). That section of river begins at Lewiston Dam and extends about 40 river miles downstream to the North Fork Trinity River (Figure 1).

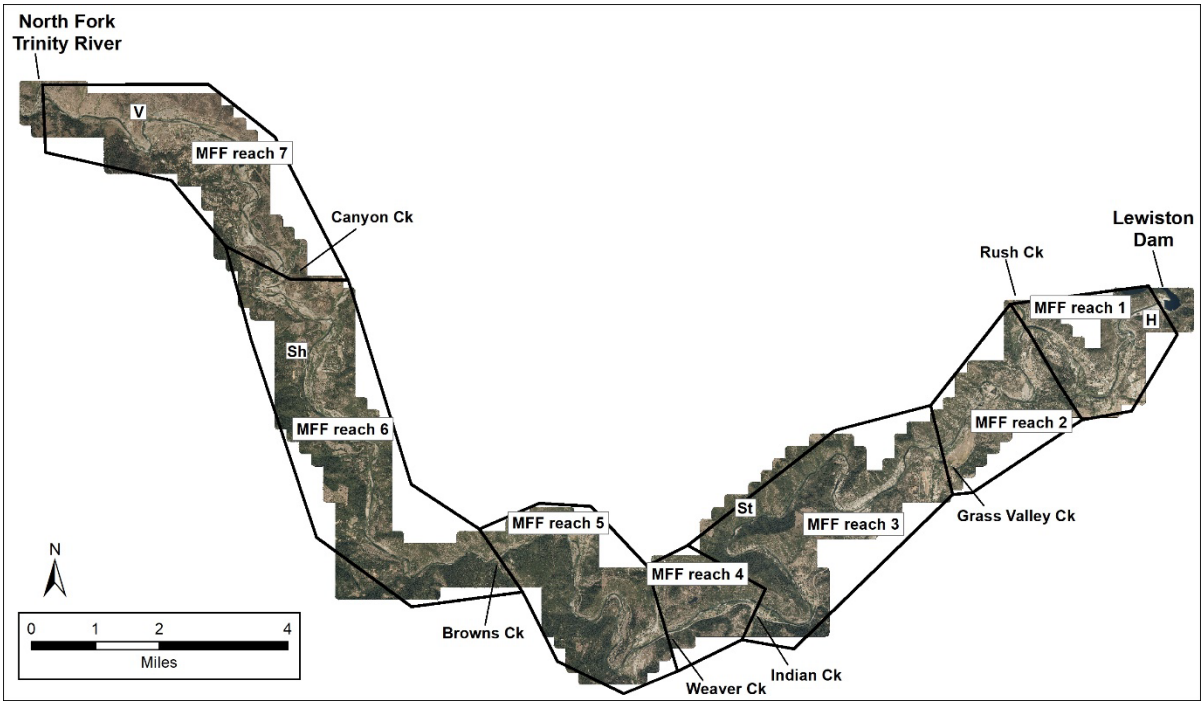

Figure 1: Locations of the seven MFF stream segments between Lewiston Dam and the North Fork Trinity River.

Hydrology

Because river discharge in the study area is regulated by Lewiston Dam, hydrologic conditions vary significantly with distance from the dam. Discharge in the immediate vicinity of the dam is entirely determined by managed flow releases. As dam operating protocols prohibit intentional release greater than 11000 ft^3/s, peak discharge at Lewiston can exceed that magnitude only due to an unscheduled release. This last occurred in spring 2017 when an instantaneous peak discharge of 12000 ft^3/s was briefly attained before operators re-adjusted flow to 11000 ft^3/s. In the downstream half of the study area, however, tributary accretions during winter storm events can greatly exceed flows out of Lewiston Dam, resulting in significant increases in both the frequency and magnitudes of flood events in downstream reaches.

The importance of tributary accretions for TRRP management is quantified in terms of Maximum Fisheries Flows (MFF), which are defined by the maximum allowable flow release from Lewiston Dam coupled with simultaneous 100-year spring tributary accretions throughout the study area (DWR 2007). The 40-miles of river between the dam and the North Fork Trinity River is partitioned into seven MFF segments, each of which is bounded by confluences with

major tributaries. The MFF associated with those segments range from 11000 ft^3/s in segment 1 just downstream from the dam to 23207 ft^3/s in segment 7, located between Canyon Creek and the North Fork Trinity River at the downstream end of the study area (Figure 1, Table 1).

To more completely describe the scale of the potential differences between the magnitudes of floods one must also include consideration of winter storms. Such storms are summarized below with estimates of the 10-year flood, as that event is relatively large and frequent. The 10-year flood is projected to be 80% to as much as 180% larger in segment 7 than it is in segment 1, depending on the estimation method used. Estimates based on fitting gage records to a Log-Pearson type III probability distribution (USGS 1981) made use of either the portion of the gage records available since modern dam operation began after the Record of Decision (USDOI 2000) was issued (segments 1, 3, and 5) or the full period of record (segments 6 and 7). The record for segment 7 only extends back to 2005, but the record for segment 6 begins in 1995. For segment 6, we chose to include peaks that occurred before modern spring flow releases were implemented because that stream segment is far enough downstream that the majority of annual peaks (15 of the 26 years) are associated with winter storm events rather than releases from the dam. We also note that the period of record at that gage (USGS 11526250) lacks measured peak discharges for two years when that gage was not in operation. The missing records were filled in with estimates obtained by correlation with the Trinity River gage near Burnt Ranch. The methods used to compute the FEMA estimates for the 10-year event are not described in that report, which only alludes to the use of watershed attributes such as area, shape, and land use (FEMA 2016).

Table 1: MFF stream segments defined within the TRRP rehabilitation domain. *Event magnitude estimated by fitting gage record to Log-Pearson type III probability distribution. ^{F}Event magnitude according to FEMA (2016). Gages identified by USGS gage numbers.

Segment	MFF (ft^3/s)	10-yr event (ft^3/s)	Gage and Records Used*	Segment Boundaries
1	11000	10910*, 11000 ^{F}	11525500, 2000-2020	Lewiston Dam to Rush Creek
2	12096	11090 ^{F}	Not available	Rush Creek to Grass Valley Creek
3	13692	11810*, 12940 ^{F}	11525655, 2003-2020	Grass Valley Creek to Indian Creek
4	15771	15360 ^{F}	Not available	Indian Creek to Weaver Creek
5	17544	12700*, 20180 ^{F}	11525854, 2003-2020	Weaver Creek to Browns Creek
6	21336	18280*, 25070 ^{F}	11526250, 1995-2020	Browns Creek to Canyon Creek
7	23207	19910*, 31150 ^{F}	11526400, 2005-2020	Canyon Creek to North Fork Trinity

The longitudinal hydrological differences summarized in Table 1 are highly relevant to the assessment of bed disturbance undertaken herein because they demand that different ranges of discharge must be considered in different parts of the study area. It is also likely that different flood magnitudes may produce differences in channel form or substrate organization that influence how and where fish use available spawning resources.

Data and Methods

Potential for flood events to entrain stream bed sediments can be evaluated by comparing sediment particles sizes present in local areas within the channel with the fluid forces generated by a range of moderate to high discharges. The potential for general bed disturbance can further be extended to an evaluation of the potential for stream bed erosion to attain depths sufficient to scour egg pockets within salmonid redds by comparing particle size and shear stress information with the locations of salmon redds. These comparisons require three sets of spatially explicit information. First, a means for estimating fluid forces throughout the stream channel is necessary. That requirement is fulfilled for this study using a 2-dimensional hydraulic model. Second, detailed information regarding the spatial distribution of sediment particles sizes on the surface is necessary. Finally, an assessment of how bed disturbance might impact salmon redds clearly requires knowledge of the precise locations where salmon redds are found.

Hydraulic Model

We estimated shear stresses using SRH-2D (Lai 2010), a 2-dimensional hydraulic model developed at the Bureau of Reclamation's Technical Services Center (TSC). This modeling platform has been used for rehabilitation site design and analysis on the Trinity River for more than a decade. Model outputs include shear stress at the stream bed in addition to several other standard hydraulic variables such as flow depth, flow velocity vectors, Froude number, etc. The particular implementation of SRH-2D used in this study spans the full valley floor over the 40-miles of the Trinity River between Lewiston Dam and the North Fork Trinity River. Created and calibrated under contract with the TSC (Bradley 2018), this model implementation represents conditions in the river at the end of water year 2016. The topographic data used to define stream morphology in the model was obtained as part of a major mapping effort that included multi-beam sonar, single-beam sonar, airborne LiDAR, structure-from-motion (SfM) photogrammetry, and conventional ground surveys. Those data and the model they support are widely used throughout the TRRP science program and are well documented elsewhere (GMA 2017; Gaeuman et al 2017; Gaeuman et al. 2019).

The model was used to estimate shear stresses in the river channel at 12 discharges between 4000 ft^3/s and the maximum MFF within the study area. The smallest modeled discharge (4000 ft^3/s) is near the threshold discharge needed to initiate gravel transport in the Trinity River (Gaeuman et al. 2017), whereas the maximum MFF in stream segment 7 is 23207 ft^3/s. Modeled discharges between those extremes are 5000, 6000, 8500, 11000, 12096, 13692, 15771, 16000, 17544, and 21336 ft^3/s (Table 2). Discharges of 11000 ft^3/s can be released directly from Lewiston Dam, whereas 6 of the 7 largest discharges correspond to MFFs defined for different portions of the 40-mile study area. For each stream segment, only those discharges less than or equal to the local MFF are considered in the analyses that follow.

Model output consists of flow depth, flow velocity, shear stress, and other hydraulic variables assigned to the centroid point of each model element at each discharge level. The smallest scale at which these hydraulic variables can be evaluated in this study is therefore determined by the size of the mesh elements that comprise the 2016 Trinity River 40-mile hydraulic model. Mesh elements within the channel where salmon spawn and where bedload transport is concentrated range from 20 to about 100 ft^2 in area, with the smallest elements being located near the channel margins (Bradley 2018).

Table 2: Discharges modeled with SRH-2D used to assess shear stresses in this study.

Q (ft^3/s)	Significance
4000	Approximate initiation of coarse bedload transport
5000	Approximate threshold for significant bedload transport
6000	Nominal normal year spring flow release from Lewiston Dam
8500	Nominal wet year spring flow release from Lewiston Dam
11000	Maximum authorized spring flow release from Lewiston Dam
12096	MFF in stream segment 2 (Rush Ck to Grass Valley Ck)
13692	MFF in stream segment 3 (Grass Valley Ck to Indian Ck)
15771	MFF in stream segment 4 (Indian Ck to Weaver Ck)
16000	Approximately the 8- and 6-yr events in segments 6 and 7, respectively
17544	MFF in stream segment 5 (Weaver Ck to Browns Ck)
21336	MFF in stream segment 6 (Browns Ck to Canyon Ck)
22000	10- to 15-yr event in stream segment 7
23207	MFF in stream segment 7 (Canyon Ck to North Fork Trinity River)

Assessing Substrate Mobility

The fluid forces that entrain sediment particles on a stream bed are normally quantified in terms of shear stress (τ), which is among the hydraulic variables output by SRH-2D. Shear stress alone, however, does not determine whether sediment particles will be entrained and transported, as the entrainment of larger particles tends to require larger shear stresses. Thus, sediment mobility is almost universally expressed in terms of a dimensionless version of shear stress given by:

$$\tau^* = \tau / \rho g R D_{50} \qquad (1)$$

where ρ is the density of water, g is acceleration due to gravity, R is the submerged specific gravity of the sediment, and D_{50} is the median particle size on the surface of the stream bed (Buffington and Montgomery 1997). A few authors prefer to use the geometric mean particle size on the stream bed (D_g) to compute τ^* (Parker 1990), but in either case the object is to characterize the particle size distribution in terms of its central tendency.

Following May et al. (2009), we define four ranges of τ^* to represent the degree of substrate disturbance and potential for scouring salmonid redds at each modeled discharge. We assume that the stream bed is static when $\tau^* < 0.03$. Values of τ^* greater than 0.03 but less than 0.045 correspond to incipient bedload transport with minor bed disturbance. Values of τ^* between 0.045 and 0.06 correspond to moderate bedload transport rates characterized by partial transport conditions (Wilcock and McArdell 1993), and $\tau^* > 0.06$ is associated with a fully mobile stream bed over which all particle sizes are in transport, high transport rates, and the potential for deep bed scour. In addition to having been defined in this way for previous studies of bed disturbance in the Trinity River (May et al. 2009), similar threshold values of τ^* for particle entrainment, partial transport, and full mobility in gravel-bed rivers are common in the geomorphic literature (Andrews 1983; Andrews and Erman 1986; Lisle et al. 2000). Of critical importance for estimating τ^* is the availability of accurate and spatially explicit estimates for D_{50} throughout the study domain. The source of D_{50} estimates used for computing τ^* is taken up next.

Stream Bed Substrate

We used a substrate map developed by TRRP agencies (Alvarez et al. 2015) as a starting point for characterizing the surface of the stream bed throughout the 40-mile study area. Data collection for the map was conducted in summer 2014 by a crew that snorkeled the entire length of the river visually estimating the 84th-percentile grain size (D_{84}) at an average of 35 point locations per 100 m of stream length. Those point estimates along with occasional polygon patches of areas composed of sand or bedrock were then interpolated to a continuous triangular irregular network surface in ArcMap. The D_{84} particle size was chosen as the mapping parameter because the map was originally intended to support estimation of roughness coefficients employed in the 2016 hydraulic model described above. Contracted staff at the TSC converted the mapped D_{84} values to Manning's n using a Manning-Strickler formulation (Ferguson 2007) that relates roughness to the 1/6 power of the D_{84} grain size. Those initial roughness values were assigned to the SRH-2D model mesh, then adjusted to optimize agreement with observed water surface elevations during model calibration (Bradley 2018).

The spatial extent of all analyses presented herein is identical regardless of discharge level used to compute τ^*. The first constraint on spatial extent is due to the lateral extent of the 2014 substrate map, which was confined to the area inundated by a discharge of about 2000 ft^3/s. All discharges for which τ^* is evaluated inundate areas beyond the limits of the substrate map, but those areas are excluded from consideration. Also excluded are areas beyond the active channel bed that remains wetted for significant durations during the winter and spring months when salmonids spawn and their eggs are incubating in the river, as portions of the stream bed that are frequently emergent at that time are irrelevant to the ecological issues that motivate this study. Although the discharges associated with particular inundation durations vary with longitudinal position along the river, the rate at which inundated area changes with changing discharges near baseflow is relatively small. We therefore chose to define the inundation footprint of our study area with a single modelled discharge of 600 ft^3/s, which we believe represents a reasonable compromise between smaller winter baseflows near Lewiston Dam and larger winter baseflows in downstream reaches. That discharge is exceeded about 67% of the time between January 1 and April 20 at the stream gage near the downstream boundary of segment 6 (USGS 11526250) but is typically within about 0.5 ft of water surface elevations at the minimum winter baseflow of 300 ft^3/s in segment 1. The spatial extent of our analyses is further restricted by removal of areas where Alvarez et al. (2015) mapped sand, bedrock, or boulders within the inundated footprint.

While the 2014 substrate map was useful for parameterizing and calibrating the hydraulic model, it is less than optimal for the purpose of assessing substrate entrainment. One difficulty is that the peer reviewed literature linking sediment mobility to shear stresses universally compute τ^* using the D_{50} or D_g rather than the D_{84}. For sediment mobility studies, it is therefore necessary to convert the mapped D_{84} values to D_{50} values. Analyses of multiple surface particle size distributions collected at different locations in the Trinity River indicate that their shapes can differ markedly. While the distribution functions are often (but not always) approximately log-normal, their standard deviations vary. Thus, no generally applicable conversion factor from D_{84} to D_{50} exists.

A second issue with the D_{84} map is that the D_{84} values themselves may be distorted. One of the authors of this report had conducted extensive field mapping of stream bed particle sizes in 2006

through 2009 and noticed that D_{84} values on the 2014 map tend to be smaller than observations of similar percentiles in prior years. At first, it was suspected that relatively small values of D_{84} may have arisen as the result of the interpolation between fine particles along the channel banks and the larger particles closer to the center of the channel employed in the 2014 map. Although such interpolation may contribute to error in some locations, we now believe that the apparent bias is primarily due to a misunderstanding of what constitutes a "pebble count" (Wolman 1954) substrate sample and how to visually estimate what the results of such a sample might be. For this study, we attempt to explain the source of misunderstanding about what a pebble count represents and convert D_{84} estimates from the 2014 map (hereafter denoted $D_{84(2014)}$) to D_{50} with a transformation developed by comparing the 2014 map with substrate maps from 2006-2009 and maps presented in May et al. (2009). The details of the bias associate with the map generated by Alvarez et al. 2015, the maps used for comparison, and the transformation can be found in Appendix A of this report.

Given these challenges, the performance of the transformation used to generate D_{50} throughout the study area is satisfactory. It should nonetheless be understood that individual estimates of D_{50}, and therefore individual values of τ^*, should not be regarded as being accurate regardless of particle size. The derived D_{50} and τ^* values are meaningful only in a statistical sense. That is, they are taken to approximate substrate and hydraulic conditions present in the river during the 2012-2016 time frame only when aggregated as statistical quantities based on large samples that span large regions of stream bed.

Location of Salmon Redds

Field surveys of salmonid redds in the study area have been conducted during spawning since 2002 (Chamberlain et al. 2012, Rupert et al. 2017a, Rupert et al. 2017b, Gough et al. 2019). Redds are surveyed weekly beginning in late August or early September and until mid- to late December. This period includes the majority of Chinook and coho spawning activity. GPS has been used to locate redds with sub-meter accuracy since 2009 (Chamberlain et al. 2012). Redds constructed in 2012 and 2014 were chosen for this evaluation because redd numbers were among the largest (in 2012) and smallest (in 2014) of those observed since 2009. This was done to account for density dependent differences in habitat selection. In addition, 2014 is also the year in which substrate mapping was performed, and the maximum peak flow released from Lewiston Dam between summer 2014 and fall 2012 (4590 ft^3/s) was insufficient to significantly alter the substrate from its 2012 condition.

Statistics summarizing the characteristics of redd locations are obtained by joining the redd locations to the shapefiles of SRH-2D output and substrate metrics, then exporting the attributes of those shapefiles to spreadsheet format. Conversely, statistics summarizing the characteristics of the general bed irrespective of the presence or absence of redds were obtained by randomly selecting 28733 points located anywhere within the analysis domain. The purpose of this sample, which constitutes about 5.4% of the approximately 536000 model elements within the 600-ft^3/s inundation footprint, was to reduce the computational demands and data management issues associated with very large datasets.

Results

Spatial Distribution of Substrate Statistics

Values of D_{50} obtained from the $D_{84(2014)}$ map via the transformation described in Appendix A are typically between about 41 and 111 mm (interquartile range) across the full study area, with a median value of 66 mm. The original $D_{84(2014)}$ values average about 60% larger through the central part of the particle size distribution, with a median of 103 mm and an interquartile range from 81 to 126 mm. The interquartile range of the $D_{84(2014)}$ values is therefore less than half the median $D_{84(2014)}$ particle size of the distribution, whereas the interquartile range of the derived D_{50} values is slightly larger than its median value. The relatively narrow range of the $D_{84(2014)}$ distribution was anticipated, as the area-by-number sampling approach used for the $D_{84(2014)}$ mapping effort (Appendix A) tends to increasingly underestimate the D_{84} particle size compared to grid-by-number sampling as the relative size of the largest particles present on the stream bed increases. It is also worth noting that, according to the $D_{84(2014)}$ map, the median D_{84} over the full study area is approximately equal to the 75th percentile of the D_{50} values in the transformed data. This suggests that compression of the particle size range associated with the sampling method used to map $D_{84(2014)}$ resulted in D_{84} estimates that, on average, represent a particle size somewhere between the actual D_{50} and D_{84} values.

The two particle size estimates, however, are broadly similar in terms of the longitudinal distribution of their median values through the study area (Figure 2). Both sets of estimates indicate that the particle sizes associated with their respective percentiles are smallest in stream segments 1 and 7 and largest in segment 5. The somewhat finer surface substrate in segment 1 is consistent with the fact that segment 1 has received gravel augmentations at various locations within the segment on a nearly annual basis for the past 14 years (Gaeuman 2020, Gaeuman and Stewart 2019, Gaeuman and Krause 2011). In segment 7, the somewhat finer substrate can be attributed to sediment deliveries from Canyon Creek at the segment's upstream boundary. Due to its large catchment area, steep gradient, and history of extreme geomorphic activity at its confluence with the Trinity River, Canyon Creek has long been considered the largest supplier of bed material to the Trinity River upstream from the North Fork Trinity River (Ritter 1968). The somewhat larger substrate indicated for segment 5 is logically consistent with the morphology of that section of river, which is characterized by a narrow bedrock-confined channel that offers relatively few locations where significant accumulations of mobile bed material can accumulate.

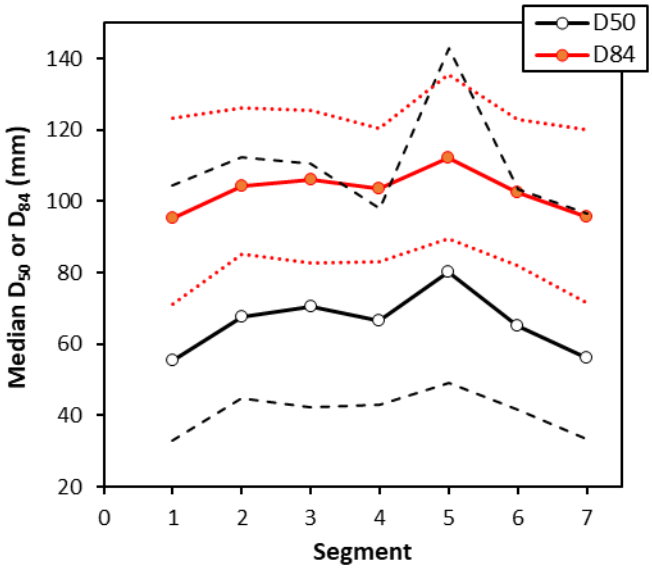

Figure 2: Median D_{50} and $D_{84(2014)}$ values within each stream segment. The thin black and red dashed lines indicate the 25th and 75th percentiles of the D_{50} or $D_{84(2014)}$ values.

These considerations lend confidence to the presumption that both the D_{50} and $D_{84(2014)}$ datasets correctly characterize trends in the spatial distribution of particle sizes on the stream bed even though the accuracy of the actual particle sizes given is uncertain. Thus, values of τ^* computed with either percentile should provide a better basis for assessing the spatial distribution of bed disturbance than can be achieved with dimensional τ. However, computing τ^* from D_{50} rather than from $D_{84(2014)}$ offers two primary advantages. First, because the sampling strategy used to create the $D_{84(2014)}$ map compresses the range of that particle size metric, the derived D_{50} estimates presumably provide a more accurate representation of the true range of substrate variability. Secondly, normalizing τ with D_{50} yields estimates of τ^* that correspond with well-defined thresholds for sediment entrainment and transport, which are generally based on Shields stresses computed with the mean or median particle size in the substrate particle size distribution.

Spatial Distribution of Redds

The longitudinal distributions of redds throughout the study area in 2012 and 2014 were similar, with stream segment 1 showing the largest absolute number and highest density of redds per unit channel length by a wide margin in both years (Figure 3). This is not unexpected as the upstream end of this segment is the limit to anadromy and the location of a large federal hatchery which produces and releases salmon and steelhead. The differences in the percentage of the total number of redds found in each segment averages 2% with a maximum difference of just 4%. We therefore conclude that neither spawner density nor water year type (i.e., normal versus critically dry) significantly influenced where salmon spawned in these years.

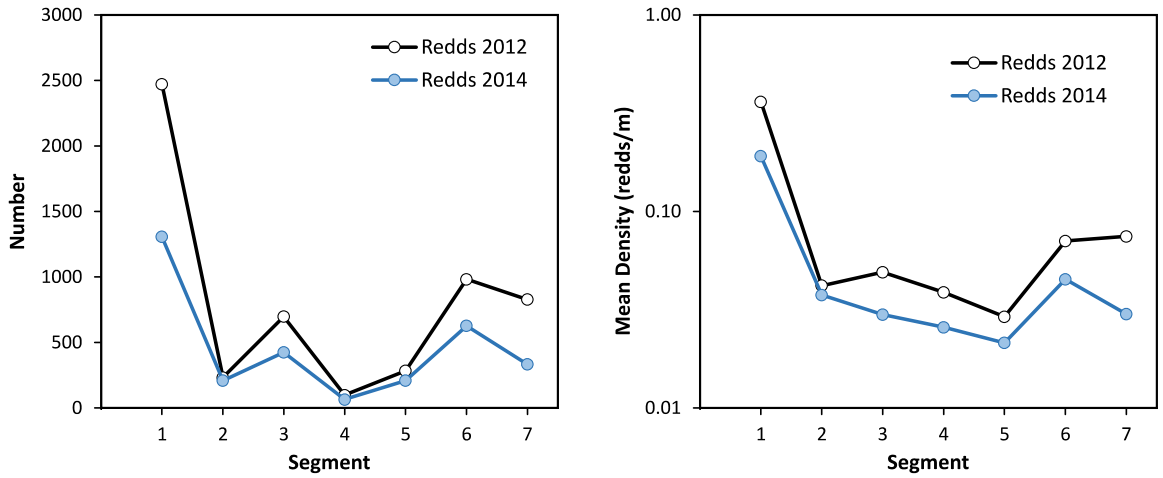

Figure 3: Numbers (left) and mean linear densities (right) of salmon redds mapped in 2012 and 2014 in each stream segment.

The preponderance of spawning in segment 1 is almost certainly a function of proximity to Lewiston Dam and the Trinity River Hatchery located immediately downstream from the dam. The linear density of redds decreases by an order of magnitude immediately downstream from segment 1 before declining more slowly to a minimum density in segment 5. As already mentioned, much of segment 5 is characterized by canyon-like morphology where substrate materials are relatively coarse and large bars are infrequent. Spawning activity picks up again in segment 6 and in segment 7, especially in 2012 when linear densities in both segments were exceeded only in segment 1. Reasons for the increase in redds per unit channel length in the downstream portion of the study area are uncertain, but it is relevant to this investigation to note that the increased magnitudes of winter floods in that part of the river (Table 1) does not appear to deter salmon spawning.

Mean Values of τ and τ^* by Discharge and Stream Segment

Plots of dimensional τ as functions of discharge for each stream segment reveal a consistent tendency for the rates at which τ increases with increasing discharge to decline as discharge exceeds 8500 ft^3/s (Figure 4). Only the curve for segment 1 lacks a clear inflection toward a flatter slope at that discharge. Most of the curves are broadly similar in shape and magnitude, with τ for most discharges being within 10% of the group mean. The curve for segment 5, however, presents an exception to this generalization in that its values of τ are 18% to 24% larger than the means of the other six segments at similar discharges. The segment 5 curve is also unique in that, after flattening at 8500 ft^3/s like most of the other curves, it regains a steep slope at discharges greater than 11000 ft^3/s.

Plots of τ^* as functions of discharge in each stream segment exhibit characteristics similar to those of the dimensional curves, in that all curves except for segment 1 show a marked inflection to lower slopes at 8500 ft^3/s (Figure 5). The relative magnitudes of some of the τ^* curves, however, are shifted from the positions of the τ curves. In particular, the curve for segment 5, which shows the largest values of τ, is shifted downward to join a tightly packed cluster of

curves representing segments 1, 2, 3, 4, and 6 through most of its discharge range. Only at its maximum flood of 17544 ft^3/s does curve 5 separate from that cluster. Curve 7, on the other hand, is shifted upward to values of τ^* that are 21% to 27% larger than the group means. The downward shift in the τ^* curve for segment 5 relative to the position of its τ curve is due to the fact that the substrate in segment 5 is characterized by larger median particles sizes than any of the other five segments (Figure 2). Likewise, the upward shift of the τ^* curve for segment 7 reflects the presence of finer substrate in that stream segment.

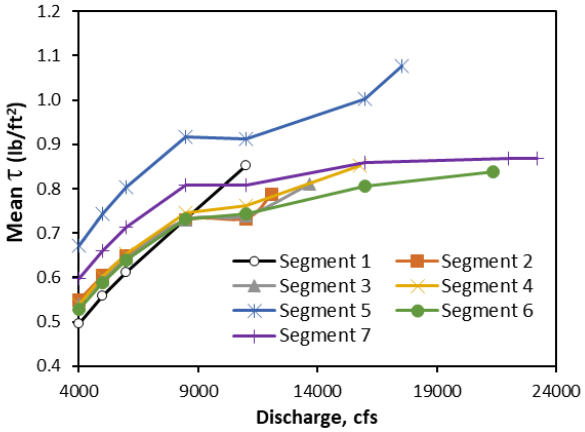

Figure 4: Mean values of dimensional τ as functions of discharge in each stream segment.

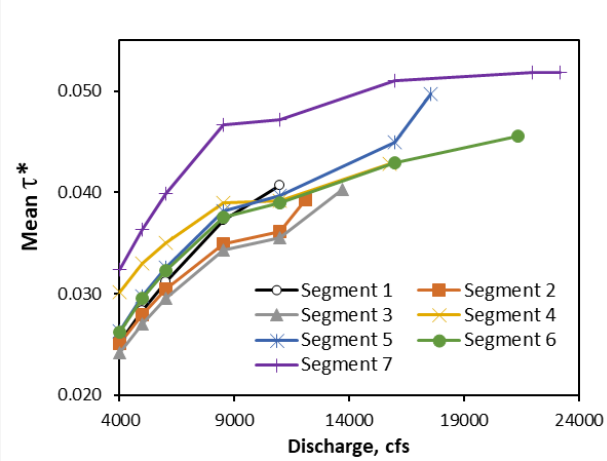

Figure 5: Mean values of τ^* as functions of discharge in each stream segment.

Extent of Bed Disturbance as a Function of Discharge

We evaluate the extent of bed disturbance as a function of discharge by computing the fraction of the stream bed where τ^* values are greater than three τ^* thresholds at each discharge evaluated (Figure 6).

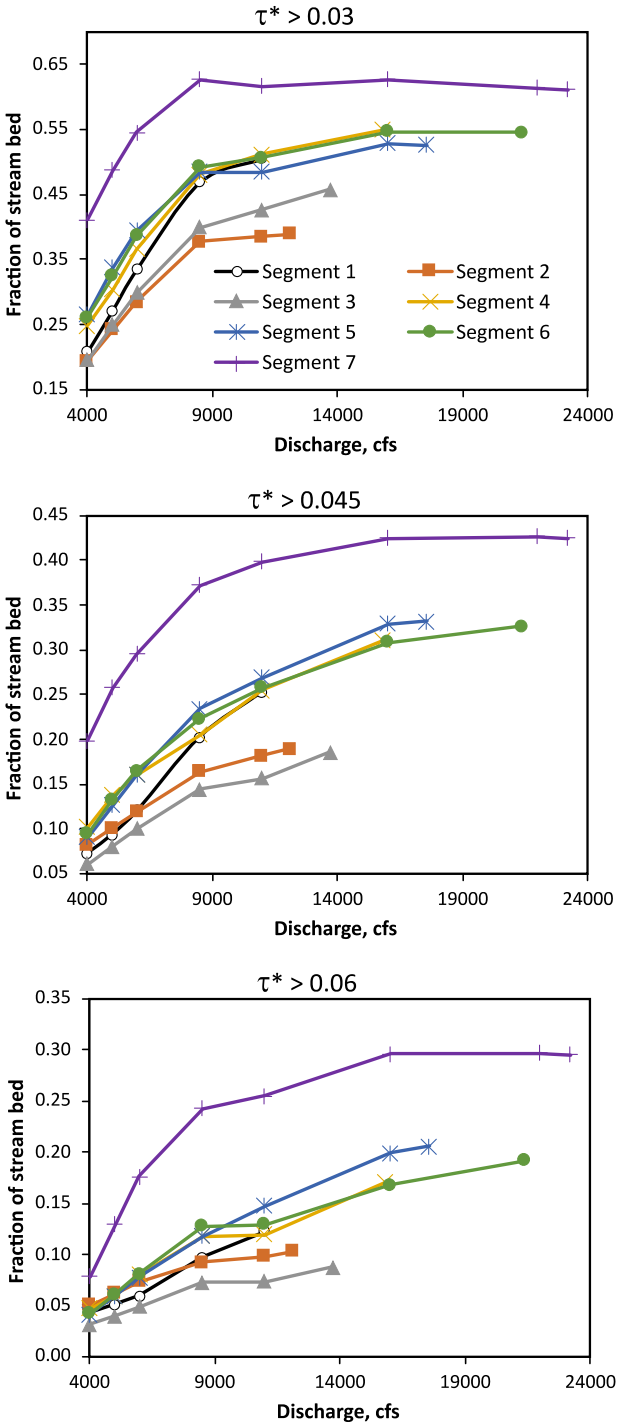

Figure 6: Fractions of the stream bed area exceeding τ^* thresholds versus discharge for each stream segment.

The presence of an inflection in the τ^* to discharge curves at or near 8500 ft^3/s noted previously is also evident in plots of the disturbed fraction of the total stream bed area within each bin over the range of discharges considered for each stream segment. For example, the fractions of the

bed with τ^* greater than 0.03 increase at rates near 0.05 per 1000 ft^3/s within the interval of 4000-8500 ft^3/s, but the slopes flatten to rates less than 0.006 per 1000 ft^3/s at larger discharges. In segment 7, the fraction of the bed with τ^* greater than 0.03 actually decreases slightly between 8500 and 11000 ft^3/s and is essentially flat thereafter. Overall, substantial fractions of the stream bed remain below the threshold of bed disturbance across the full range of flows in all segments. For segments 1 through 6, where the maximum fractions of area with $\tau^* > 0.03$ range from 39% in segment 2 to 55% in segment 4, approximately half the stream bed area remains essentially immobile during even the largest floods. That fraction is notably different only in segment 7, where the fraction of the stream bed subject to $\tau^* > 0.03$ attains 63% as discharge exceeds 8500 ft^3/s and maintains levels in excess of 61% across all larger discharges.

The $\tau^* > 0.045$ curves also tend to flatten with increasing discharge, but to a lesser extent than the $\tau^* > 0.03$ curves. The $\tau^* > 0.045$ curves for segments 1 through 6 reach maximum fractions equivalent to between a fifth to a third of the stream bed area. Again, segment 7 stands out with a substantially larger fraction of disturbed area that reaches 43% of the bed area.

Curves for the fractions of the bed with τ^* greater than 0.06 display the same general pattern as the curves for the smaller τ^* thresholds. Apart from some minor differences in the relative positions of the curves for segments 1-6 curves, they mainly differ from the 0.03 and 0.045 curves only in having smaller maximum magnitudes. For segments 1-6, the maximum fractions of the stream bed that experiences $\tau^* > 0.06$ range from 9% in segment 3 to 21% in segment 5, whereas the curve for segment 7 reaches a maximum of 30%.

Discharge-to-τ^* Relationships at Redd Locations

Comparisons between mean values of τ^* over the full stream bed area with mean values of τ^* where salmon redds were located in 2012 and 2014 show that redds tend to be restricted to a narrower range of τ^* than is generally available within the baseflow channel where salmonids spawn (Figure 7). Mean values of τ^* at 4000 ft^3/s for redd locations in either year (i.e., the minimum mean values across the range of discharges) are similar to τ^* averaged over the full stream bed, whereas the mean values of τ^* reached at 11000 ft^3/s (i.e., the maxima displayed in Figure 7) are about 20% smaller at redd locations than over the full stream bed. Discharges larger than 11000 ft^3/s are neglected for this comparison of means, as the larger discharges that are possible in downstream segments are not applicable to the more upstream segments. Besides demonstrating the more moderate mean values of τ^* typical of redd locations, this comparison is intended to demonstrate that the hydraulic characteristics of redd locations mapped in 2012 are virtually indistinguishable from the locations mapped in 2014. Having established that the τ^*-to-discharge characteristics of redd locations mapped those two years are substantially similar, we combine the redd locations from both years for analyses presented below.

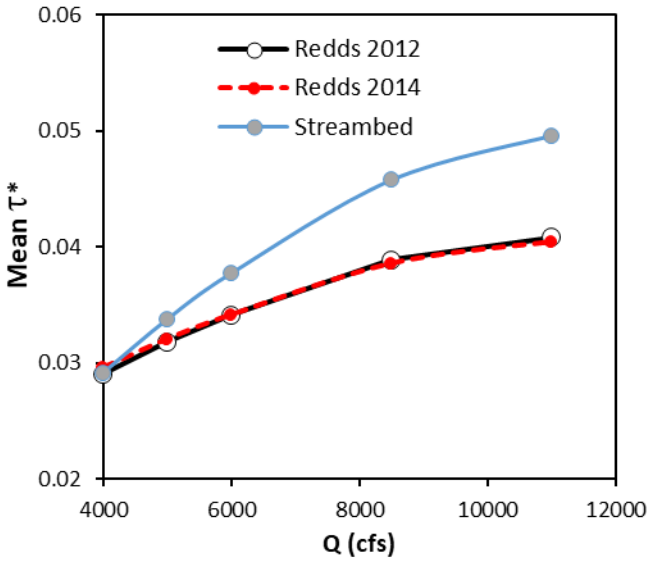

Figure 7: Mean values of τ^* versus discharge for redd locations in 2012, redds locations in 2014, and the overall stream bed as a function of discharge.

Evaluating differences in mean values of τ^* can be misleading because values of τ^* for neither the full stream bed nor redd locations conform to a normal probability distribution. The smallest values of τ^* are necessarily bounded at zero, but τ^* can attain arbitrarily large values in local areas with large τ and/or small substrate. This leads to positively skewed frequency distributions with large outliers that can significantly bias their mean values (Figure 8). An evaluation of these differences based on percentiles suggests that the large difference between mean values of τ^* for redds versus the stream bed area as a whole is primarily driven by a tendency for spawners to avoid areas with especially large τ^*. Over the full study area, the majority (75%) of the stream bed area and the majority of redd locations experience values of τ^* that remain below 0.05 over the full range of discharges that occur in all stream segments (Figure 9, panel A). However, spawners also appear to avoid areas with especially low τ^*, as shown by the 25th percentile of τ^* values, which for redd locations are about 20% larger than the 25th percentile for the stream bed across the same discharge range. An apparent preference on the part of spawners for locations that experience moderately high τ^* is also suggested by the fact that both the median and the 75th percentile values of τ^* are consistently larger for redd locations than for the stream bed, especially at smaller discharges when all τ^* percentiles are smallest.

The apparent avoidance of areas with small τ^* on the part of spawners results in a tendency for the range of τ^* values at redd locations to be narrower than the range of τ^* present over most of the stream bed. When calculated independently for each stream segment, the interquartile range of τ^* for the stream bed is between 13% and 56% larger than the interquartile range at redd locations in 6 of the 7 stream segments (Figure 9, panel B). Only in segment 3 are the ranges for redd locations and the general stream bed approximately equal.

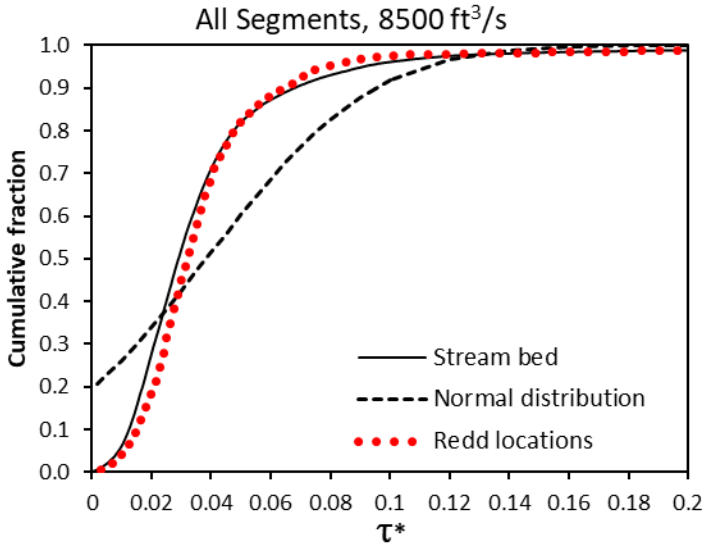

Figure 8: Cumulative frequency distributions of τ^* over all stream segments and at all redd locations at 8500 ft^3/s. The dashed black line shows the plotting position of a normal frequency distribution with the same mean and standard deviation as the curve for the stream bed.

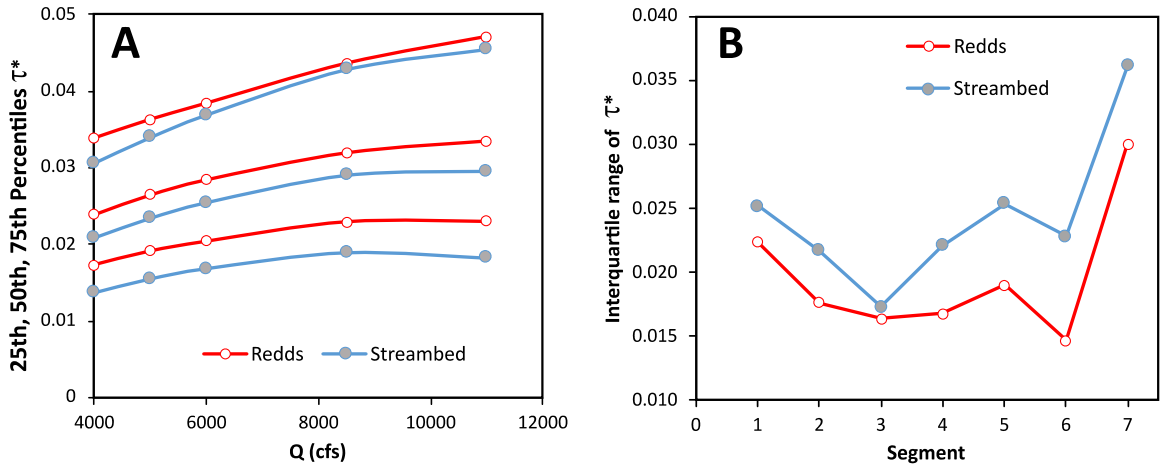

Figure 9: A) 25th, 50th, and 75th percentiles of τ^* over the full stream bed and at redd locations mapped in 2012 and 2014. The discharge range plotted is restricted to 4000 to 11000 ft^3/s. B) Interquartile ranges of τ^* at 8500 ft^3/s for the general stream bed and for all redd locations in each stream segment.

Bed Disturbance at Redd Locations

Plots of the fraction of redds located in areas with τ^* values exceeding the τ^* thresholds previously defined for bed disturbance (Figure 10) show substantially more between-segment variability, as well as greater within-segment variability for many segment-threshold combinations, than do the corresponding plots for the general bed disturbance (Figure 10 and Figure 6 are plotted using the same vertical scales to facilitate comparison).

In keeping with the earlier observation that spawners may avoid areas where τ^* is much smaller than the threshold for bed entrainment during small to moderate flood events, the fraction of redd locations where τ^* exceeds 0.03 at 4000 ft^3/s over the full study area is 34% larger than the corresponding fraction for the general stream bed. At the local scale, the fraction of redd locations with $\tau^* > 0.03$ at 4000 ft^3/s is greater than the fraction for the stream bed in five of the seven stream segments, with the relative differences ranging from 5% in segment 5 to 77% in segment 3 (Figure 11, panel A). In the remaining two segments (segments 4 and 6), however, the fraction of redd locations with $\tau^* > 0.03$ at 4000 ft^3/s is 29% and 16% smaller than over the general stream bed. The somewhat contrary result for segment 4 may be related to a lack of morphologic diversity and/or a scarcity of redds in that segment. Defined by the confluences of Indian Creek and Weaver Creek, segment 4 consists of a straight section of river less than 1.5 miles long (Figure 1). Moreover, the number of redds counted within the segment – 98 in 2012 and 65 in 2014 (Figure 3) – may not represent an adequate sample size. No similar explanation for the relatively small fraction of redd locations with $\tau^* > 0.03$ at 4000 ft^3/s in segment 6 is apparent.

In addition to beginning at larger fractional values at 4000 ft^3/s, many of the $\tau^* > 0.03$ curves rise steeply with increasing discharge and attain larger maximum values than the stream bed curves. In particular, the segment 1 redds curve rises to the largest absolute fraction of $\tau^* > 0.03$ of any segment for either the redd locations or the stream bed (Figure 11, panel B).

The anomalously steep rise in the segment 1 redds curve for $\tau^* > 0.03$ is even more exaggerated in the segment 1 redds curve for $\tau^* > 0.045$. That curve maintains a constant steep slope over its full discharge range and attains a maximum value that clearly exceeds all other redds curves (Figure 10) and is 54% larger than the corresponding curve for the general stream bed. All but one of the remaining $\tau^* > 0.045$ curves for redd locations attain peak values similar to or larger than curves for the general stream bed. Only in segment 6 does the redds curve for $\tau^* > 0.045$ remain below the maxima attained by the stream bed curve. This apparent propensity for redds to be located in areas that can exceed $\tau^* = 0.045$ is consistent with the hypothesis that spawners prefer, or at a minimum do not avoid, areas likely to experience moderate levels of bed mobility.

In contrast to the relatively large fractions of redd locations that exceed the 0.03 and 0.045 thresholds, relatively small fractions of redd locations experience $\tau^* > 0.06$. Few of the redds curves for $\tau^* > 0.06$ rise far above their initial values at 4000 ft^3/s. The redds curves for segments 3 and 6, for example, respectively begin at 0.055 and 0.025 but reach respective maxima of just 0.084 and 0.074 (Figure 10). The general bed curves, in contrast, show consistent increases in τ^* through at least 8500 ft^3/s. The segment 1 curve for redd locations again stands out with a consistently steep rise across the full range of possible discharges, ultimately rising to a level 68% greater than the corresponding curve for the general stream bed (compare Figure 10 to Figure 6), whereas the other six stream segments reach maximum fractions similar to or substantially less than the fraction attained by the stream bed curves (Figure 11, panel C).

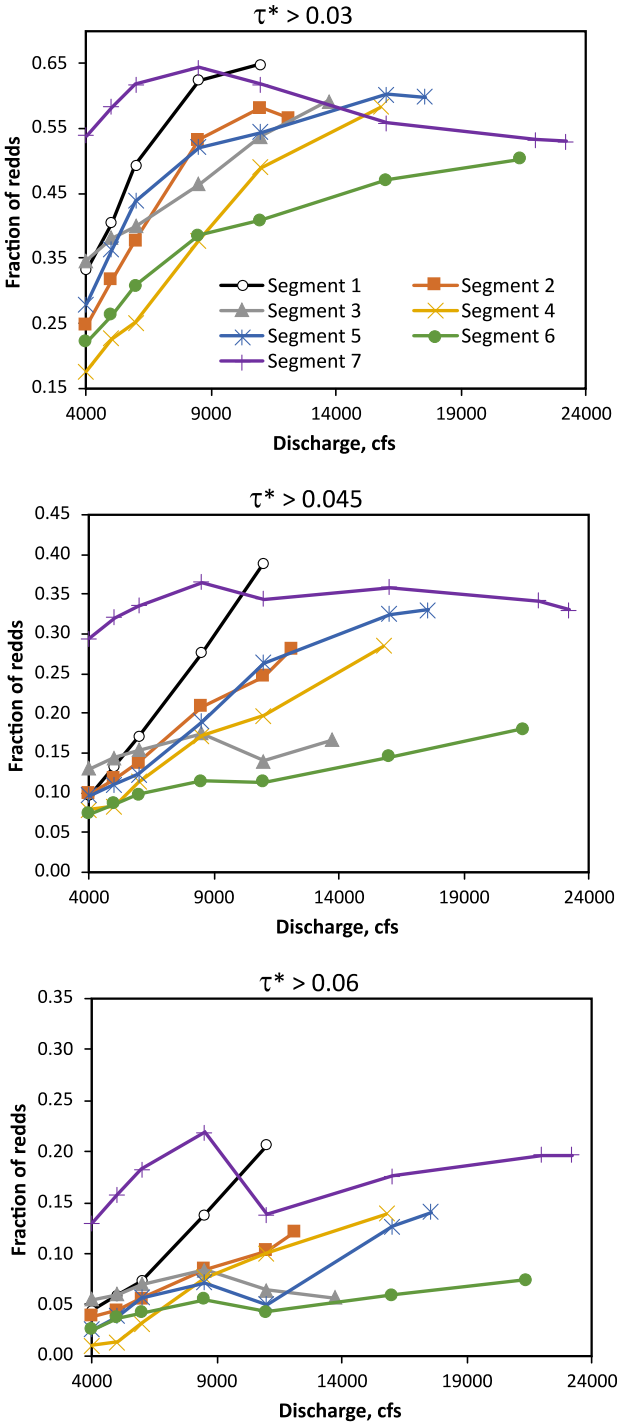

Figure 10: Fractions of redd locations exceeding τ^* thresholds versus discharge for each stream segment.

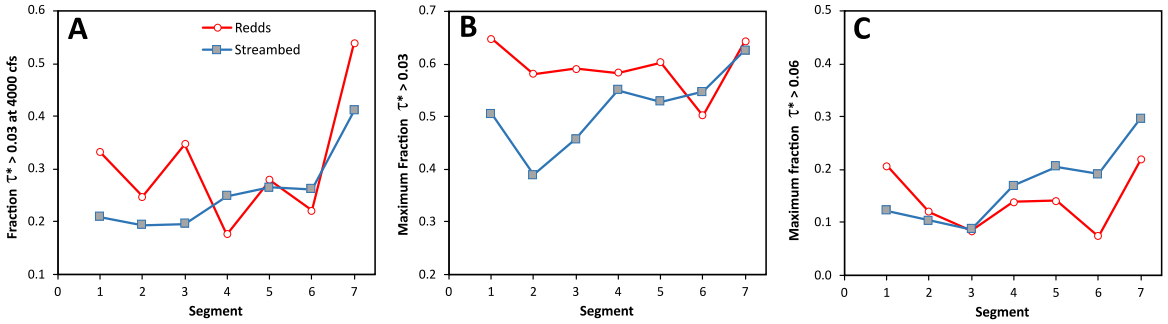

Figure 11: Comparisons between A) the fractions of redd locations and the general bed area where $\tau^* > 0.03$ at 4000 ft^3/s, B) the maximum fractions exceeding $\tau^* = 0.03$ at any discharge, and C) the maximum fractions exceeding $\tau^* = 0.06$ at any discharge in each stream segment.

It is important to note that the redds curves also differ from the curves for the stream bed in having more frequent and much larger slope reversals. Substantial reversals can be seen, for example, in the $\tau^* > 0.06$ redds curves for segments 3, 4, and 5, and in the curves for all three threshold levels in segment 7 (Figure 10). That is, shear stresses at some locations in the stream can decrease as discharge increases. Moreover, shear stress reversals appear to be more prevalent at redd locations than they are over the stream bed at large.

Further investigation of the shear stress reversals evident in Figure 10 requires element-by-element tracking of variations in τ^* with respect to discharge to quantify the phenomenon over the course of a flood hydrograph. We evaluate this aspect of change in τ^* with respect to discharge with the aid of the following variables: F_{P03} is defined as the fraction of the stream bed or of redd locations that attains $\tau^* > 0.03$ at some discharge and persists above that threshold at all larger discharges and F_{R03} denotes the fraction of the stream bed or redd locations that attains $\tau^* > 0.03$ at some discharge but reverses the direction of change to fall back below that threshold at some larger discharge. The proportion of the stream bed area or of redd locations where τ^* exceeds 0.03 but then decreases to a value smaller than that threshold is given as a percentage by:

$$R_{03} = 100F_{R03}/(F_{R03} + F_{P03}) \qquad (5a)$$

quantifies the total fraction that attains $\tau^* > 0.03$ at any discharge up to the maximum evaluated for each stream segment. Similarly:

$$R_{045} = 100F_{R045}/(F_{R045} + F_{P045}) \qquad (5b)$$
$$R_{06} = 100F_{R06}/(F_{R06} + F_{P06}) \qquad (5c)$$

are defined for the thresholds corresponding to partial mobility ($\tau^* > 0.045$) and full bed mobility ($\tau^* > 0.06$). Because these variables can be efficiently computed with merged data from any stream segments that share a common number of modeled discharges, they are presented in terms of stream segment groups rather than as individual segments. Thus, two groups are created by combining data for segments 2-4 and data for segments 5-6, whereas segments 1 and 7 remain separate.

Data tabulated into these four stream segments groups show that F_{R03} computed for the overall stream bed ranges from 0.037 to 0.117 (Table 3). R_{03} accounts for 6.9% of the stream bed area that exceeds the threshold of entrainment in segment 1, but that percentage increases in the downstream direction to 16.3% in segment 7 as the range of possible discharges increases. Similarly, R_{045} comprises 9.6% of the stream bed area that exceeds $\tau^* = 0.045$ in segment 1 and increases to 18.0% of in segment 7, whereas R_{06} ranges from 13.0% in segment 1 to 20.5% in segment 7.

Table 3: Proportions of the stream bed where τ^* thresholds are exceeded and of shear stress reversals in stream segment groups subject to similar discharge ranges. See text for explanation.

Segment	F_{P03}	F_{R03}	R_{03} (%)	F_{P045}	F_{R045}	R_{045} (%)	F_{P06}	F_{R06}	R_{06} (%)
1	0.504	0.037	**6.9**	0.252	0.027	**9.6**	0.122	0.018	**13.0**
2-4	0.444	0.066	**13.0**	0.198	0.036	**15.3**	0.099	0.019	**16.0**
5-6	0.527	0.076	**12.6**	0.316	0.051	**13.8**	0.183	0.034	**15.9**
7	0.599	0.117	**16.3**	0.523	0.115	**18.0**	0.390	0.101	**20.5**

These findings indicate redds are preferentially located in areas where shear stress reversals are more common, especially in areas that approach conditions of full bed mobility. R_{06} for redd locations can be twice as large as R_{06} for the overall stream bed (Table 4; Figure 12). Likewise, the percentage of redd locations that experience reversals across the 0.045 threshold are at least 1.85 times larger than the percentages for the bed everywhere except for in segment 1. In general, the percentages for redd locations and the stream bed are more similar for smaller τ^* thresholds and in the more upstream stream segments. R_{03}, for example, is similar to R_{03} for the stream bed everywhere except for in segment 7 where the percentage of reversals at redd locations is 1.8 times larger than the percentage for the overall stream bed.

Table 4: Proportions of redd locations where τ^* thresholds are exceeded and of shear stress reversals in stream segment groups subject to similar discharge ranges. See text for explanation.

Segment	F_{P03}	F_{R03}	R_{03} (%)	F_{P045}	F_{R045}	R_{045} (%)	F_{P06}	F_{R06}	R_{06} (%)
1	0.648	0.044	**6.3**	0.386	0.031	**7.4**	0.203	0.022	**9.8**
2-4	0.575	0.068	**10.6**	0.197	0.068	**25.6**	0.077	0.033	**30.0**
5-6	0.506	0.073	**12.6**	0.203	0.058	**22.3**	0.081	0.031	**27.6**
7	0.515	0.216	**29.5**	0.386	0.128	**24.9**	0.181	0.134	**42.5**

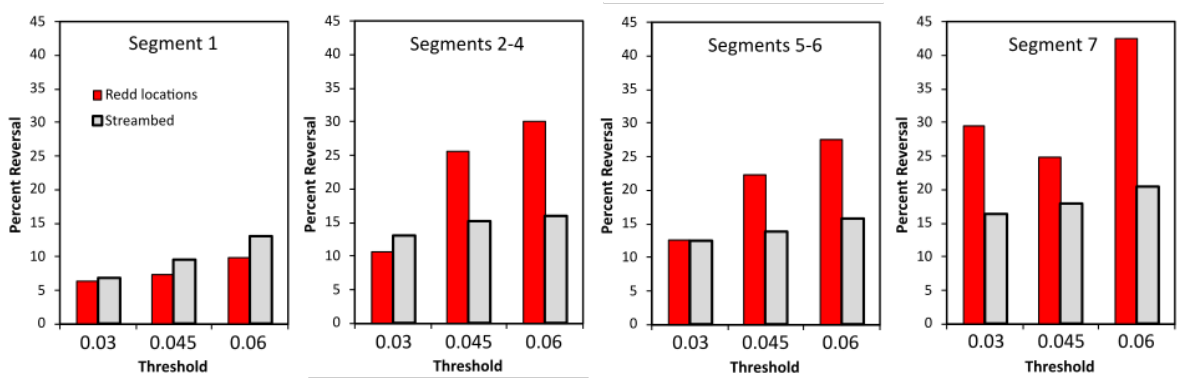

Figure 12: Graphs of R_{03}, R_{045}, and R_{06} for stream segment groups subject to similar discharge ranges.

As has already been observed with respect to other results, segment 1 stands apart from the remainder of the study area in how τ^* is distributed at redd locations versus the overall stream bed. In the context of τ^* reversals, segment 1 is unique in that τ^* reversals are less frequent at redd locations in that segment than reversals over the stream bed for all three τ^* thresholds.

Discussion

Shear Stress Reversal

The prominence of shear stress reversals at redd locations in stream segments 2 through 7 together with the relative lack of reversals in stream segment 1 suggest two lines of inquiry. First, having demonstrated that τ^* reversals are more frequent at redd locations than over the stream bed at large, it is natural to ask what mechanisms account for the reversals and why redds are associated with them. Second, it is natural to also ask why the hydraulic characteristics of redd locations in segment 1 contrast so sharply with those of redd locations elsewhere in the study area.

The greater likelihood of τ^* reversals at redd locations than elsewhere on the stream bed can be at least partially explained by noting that salmonid redds are generally found near gravel bars or riffles. Spawning riffles are, by definition, places where gravel is deposited during flow events that mobilize the stream bed. It is therefore necessary that shear stresses over riffles during floods be small enough for bedload to accumulate, even though shear stresses over riffles tends to be relatively large during baseflow periods. Keller (1971) was among the first to explicitly discuss this aspect of riffle maintenance and proposed that the location of the highest flow velocities shifts from riffle locations to pool locations as discharge increases to levels that mobilize the stream bed. Introduced as the "velocity reversal" hypothesis by Keller (1971), the idea was quickly modified to recognize a potential reversal in the locations of the higher shear stresses during floods (Lisle 1979), or at least an equalization between the shear stresses over the riffle and the pool (Carling 1991). Others have extended the idea to reversals associated with flow divergence and convergence (Cao et al. 2003; MacWilliams et al. 2006), changes in downstream backwater conditions (Pasternack et al. 2008), and lateral shifts in the position of the shear stress or bedload transport lanes (Wilkinson et al. 2004; Milan 2013). Regardless of how

one describes the details, it is clear that bars and riffles are locations where shear stresses are more likely to increase slowly with discharge or even decrease with discharge than other stream bed locations.

Bars and riffles display a wide range of sizes, morphologies, and settings within the larger stream reach. Consequently, the degree of hydraulic stability and frequency of reversals associated with individual riffles must also vary. Although much of the literature on hydraulic reversals focusses on the scale of individual bars, reversals can also be linked to valley-scale features, such as constrictions in valley width or abrupt bends in valley planform. These larger-scale features might emerge as hydraulic controls only during the largest floods as the more local controls associated with riffles and variations in channel width are "washed out." We explore the possibility that redds are preferentially located in areas where changing hydraulic controls tend to maintain shear stresses at moderate levels over a wide range of discharges by examining a small selection of local areas with relatively high concentrations of redds.

An example of where a concentrated patch of redds appear to be associated with a local-scale hydraulic control that produces shear stress reversals is located in stream segment 3 about 1600 ft upstream from the Steel Bridge river access (location labeled St on Figure 1). A relatively dense cluster of redds is mapped at the downstream end of a channel anabranch that flows around the right side of a large medial bar or island. The anabranch around the left side of the island, however, is relatively deficient in redds (Figure 13). Hydraulic model output indicates that portion of the right anabranch where the redds are concentrated begins to show shear stress reversals early in a flood hydrograph, whereas reversals are either absent in the left anabranch or fail to appear until discharge reaches 11000 ft^3/s or more (Figure 14). The map shown in Figure 14, as well as the other reversal maps that follow, depicts the first discharge at which reversal begins. Regions with no color indicate that shear stress reversals do not occur at any discharge. Areas that begin to reverse at lower discharges typically show more persistent negative trends in shear stress as a function of discharge or otherwise tend to remain relatively low across the range of discharges. Reversals at discharges of 6000 ft^3/s or less in the right anabranch appear to be due to a net decrease in channel width immediately downstream from the island. As most of the total discharge is conveyed past the island through the left anabranch, the right anabranch is partially backwatered by a water surface elevation at the confluence point that is largely imposed by flow from the left branch. As a result, maximum dimensional shear stresses to the right of the island remain within a range that only partially mobilizes gravel sizes that are suitable for spawning, whereas maximum shear stresses exceed the threshold for full mobility over much of the area to the left of the island (Figure 15).

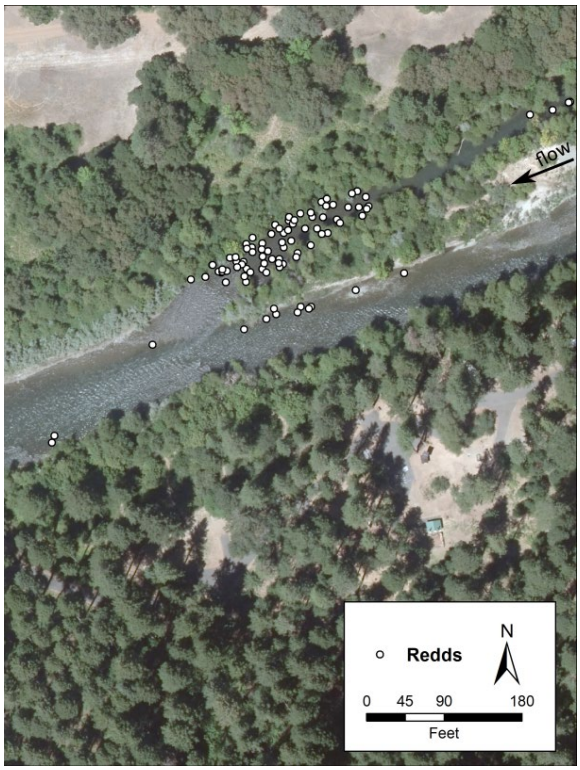

Figure 13: Cluster of redds at the downstream end of an island and flow split located 1600 ft upstream from the Steel Bridge river access.

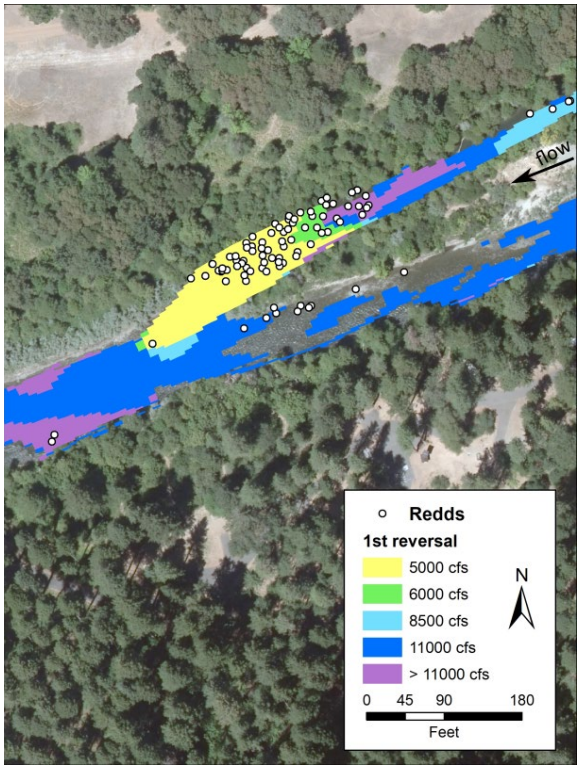

Figure 14: Map of discharges when first shear stress reversal occurs near the downstream end of the island and flow split near the Steel Bridge river access.

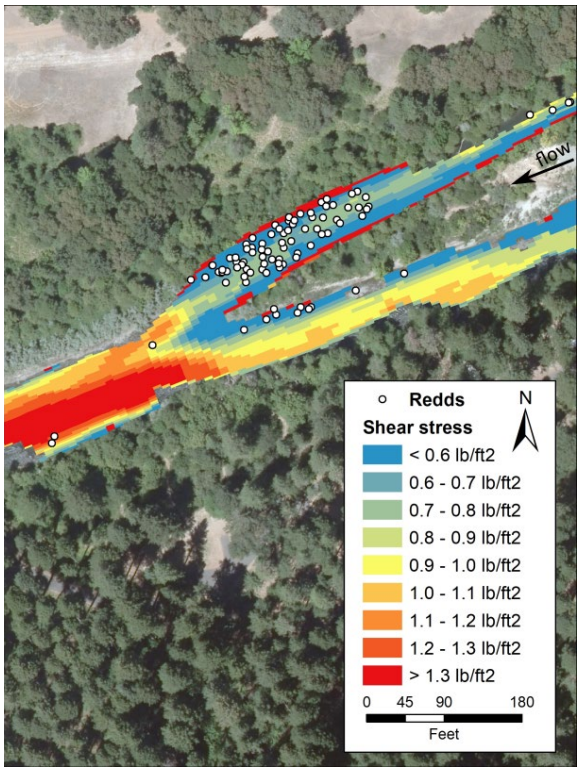

Figure 15: Map of maximum modeled shear stresses near the downstream end of the island and flow split near the Steel Bridge river access.

The color ramp in Figure 15, as well as in similar dimensional shear stress maps presented below, is scaled to correspond to thresholds of τ^* referenced to substrate with a median particle size of 60 mm. That grain size is selected as being within the range of bed material sizes suitable for salmonid spawning (Riebe et al. 2014). Dark blue (< 0.6 lb/ft^2) therefore corresponds to an assumed τ^* < about 0.03 if it is assumed that the local particle size distribution is suitable for salmonid spawning. Likewise, deep orange (1.2 – 1.3 lb/ft^2) corresponds to τ^* that exceeds 0.06 under the same particle size assumption. Use of dimensional shear stress and the assumption of suitable substrate here means that this discussion of shear stress reversals and the consequences of those reversals is independent of the 2014 substrate map or the transformation between D_{84} and D_{50} particles sizes.

Another highly concentrated patch of redds occurs along the right stream bank immediately upstream from a 90-degree bend in the river valley within the 2007 Valdor Gulch restoration project site (Figure 16). In strong contrast to the area upstream from the bend, only three redds are mapped in the vicinity of another well-developed riffle located downstream from the bend. The bend itself, which is labeled V in Figure 1, is forced by a nearly vertical bedrock valley wall on river right that appears to increasingly limit flow velocities and shear stresses in the baseflow channel upstream as discharge increases. As discharge and stage rise, an increasing proportion of flow can be conveyed over a wide point bar on the left bank, so the hydraulic control imposed by the valley wall is most effective near the right bank where most of the redds are located. Shear stress reversals beginning at 5000 ft^3/s cover most of the right half of the channel within about 200 ft of the bend apex and grades to reversals that begin at progressively larger discharges in

both the upstream and lateral directions (Figure 17). Because this location is situated in stream segment 7, the range of possible discharges extends to a MFF of 23200 ft^3/s. Due to the abundant opportunities for shear stress reversals to occur at very high discharges when much of the flow is conveyed through overbank regions, virtually the entire baseflow channel within the extents of the figure experiences a reversal at some point during a maximum flood. While the downstream riffle with three mapped redds also experiences shear stress reversals, the reversals in much of that area are delayed until discharge has exceeded 22000 ft^3/s and shear stresses have already become large (Figure 18).

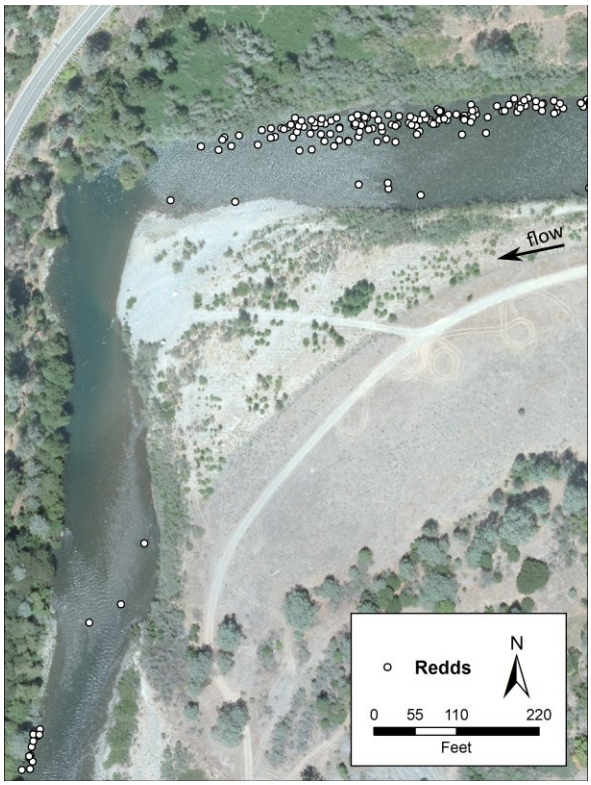

Figure 16: Cluster of redds upstream from an abrupt valley bend in stream segment 7.

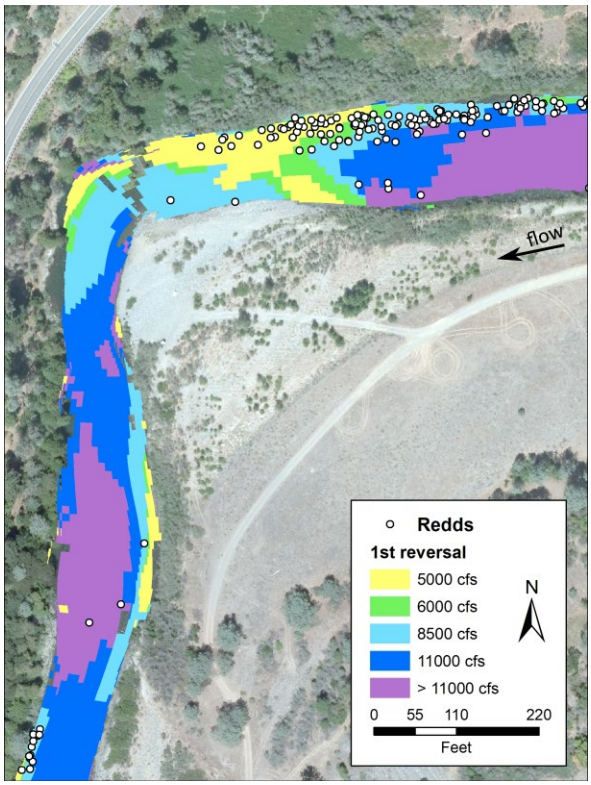

Figure 17: Map of discharges when first shear stress reversal occurs upstream from an abrupt valley bend in stream segment 7.

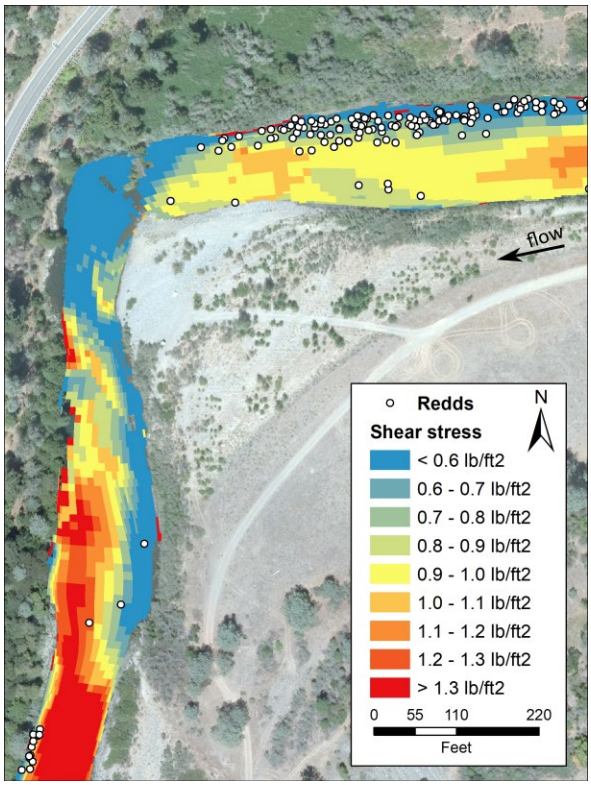

Figure 18: Map of maximum modeled shear stresses upstream from an abrupt bend in segment 7.

A third area where concentrations of redds are associated with regions of moderate shear stresses is the stream reach near the mouth of Sheridan Creek, which is located is stream segment 6 (Figure 19). This reach is widely regarded as the most heavily spawned area in the Trinity River downstream from the fish hatchery at Lewiston Dam (Rupert et al. 2017). Redds mapped in this reach in 2012 and 2014 appear in two main clusters. A more downstream cluster occupies a gravel bar immediately upstream from a bedrock outcrop with a deep hole at its base. The location of that outcrop is labeled "Sh" on Figure 1. About half of that bar and the associated cluster of redds lies within a region that begins to experience shear stress reversals at 5000 to 8500 ft^3/s (Figure 20). Reversals at relatively small flood discharges in that area appear to be related to local backwater conditions produced when flow is deflected to the right by the bedrock outcrop.

The other half of the downstream cluster of redds, however, lies in a region where reversals do not occur until discharge reaches 11000 ft^3/s or not at all. Moreover, a larger cluster of redds roughly 600 to 900 ft upstream from the bedrock outcrop lies in an area that mostly either lacks reversals or where reversals occur only at large discharges. Although the presence of abundant redds in the Sheridan reach does not appear to be related to shear stress reversals, it is nonetheless still related to factors that moderate shear stresses in the area. The water surface slope through the Sheridan spawning reach is 0.0016 (Yurok Tribe & NHE 2017), which is low compared to the average slope of the Trinity River between Lewiston Dam and the North Fork Trinity River of 0.0023 (Gaeuman et al. 2016). This low slope together with the hydraulic control imposed by the bedrock outcrop at the downstream end of the reach, as well as by other potential larger-scale controls, serve to limit maximum shear stress magnitudes to 1 lb/ft^2 or less throughout the reach (Figure 21). If the substrate in the area is assumed to be suitable for salmonid spawning with a median particle size of 60 mm, the dimensional shear stresses attained at redd locations in the reach are equivalent to τ^* between about 0.03 to 0.05. Thus, actual point reversals are not necessary to maintain shear stresses within an optimal range for salmonid spawning if the rates at which shear stresses increase with discharge are low.

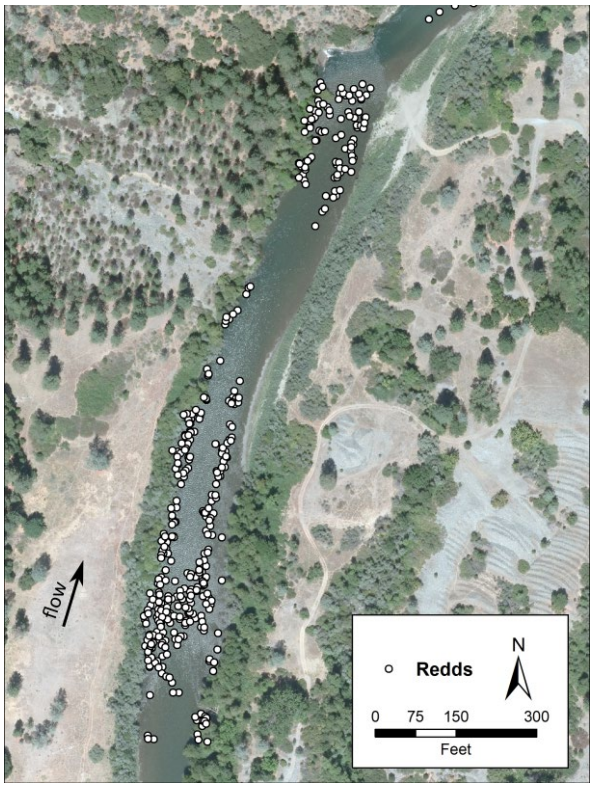

Figure 19: Clusters of redds in the Sheridan reach.

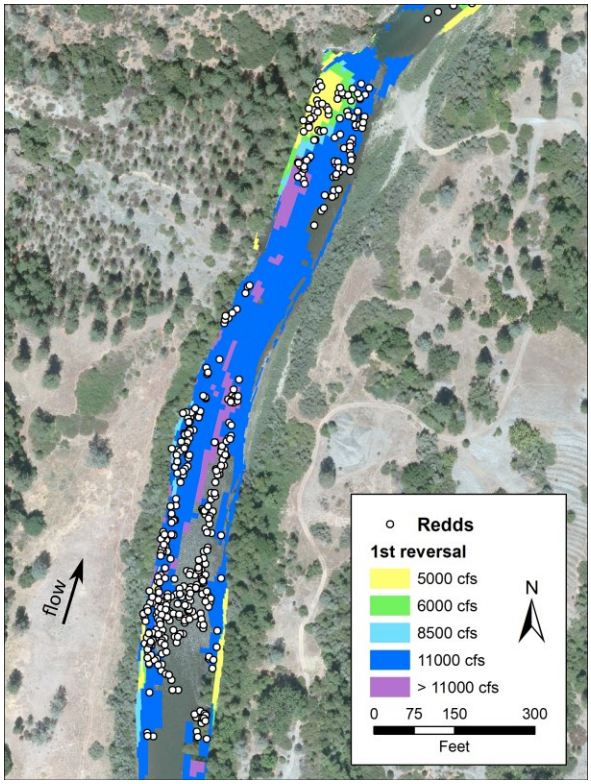

Figure 20: Map of discharges when first shear stress reversal occurs in the Sheridan reach.

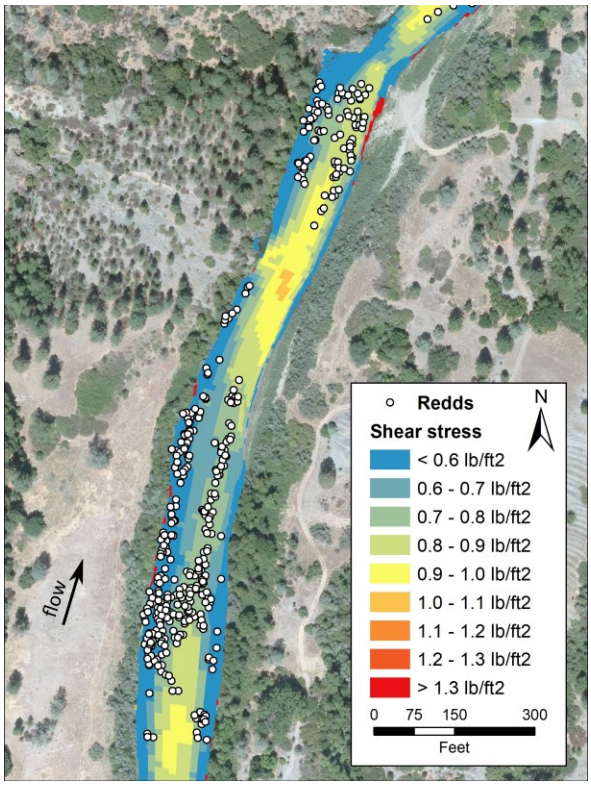

Figure 21: Map of maximum modeled shear stresses in the Sheridan reach.

Segment 1 and the Hatchery Reach

Our results regarding shear stress reversals, or lack thereof, also provide an explanation for the anomalous distributions of τ^* at redd locations in segment 1. More than 43% of the redds mapped over the full study area in 2012 and 2014 were located in segment 1. Of the 3734 redds mapped in segment 1, more than 27% are located within 2200 ft of Lewiston Dam in a straight section of channel adjacent to the Lewiston Fish Hatchery (Figure 22).

As a by-product of hatchery construction, the adjacent Trinity River channel and floodplain was replaced with a trapezoidal channel with uniform width and a planar bed. Attempts to augment spawning gravel or introduce topographic structure into the reach were suspended in 2007, and whatever benefit was gained by those efforts had been largely erased by multiple spring high flow releases before the 2016 topographic data used for hydraulic modeling was obtained. As a result, the 2016 hatchery reach lacked the topographic structure or planform variability necessary to support shear stress reversals or to moderate shear stresses as discharge increases to flood levels. Consequently, the model output is nearly devoid of shear stress reversals (Figure 23) and many mapped redds are located in unprotected locations where shear stresses are capable of fully mobilizing bed material in the spawning gravel range as discharge increases toward the maximum dam release of 11000 ft^3/s (Figure 24). The number of redds vulnerable to scour with high discharge in the artificial channel adjacent to the hatchery is sufficiently large to skew the τ^* statistics for all of stream segment 1.

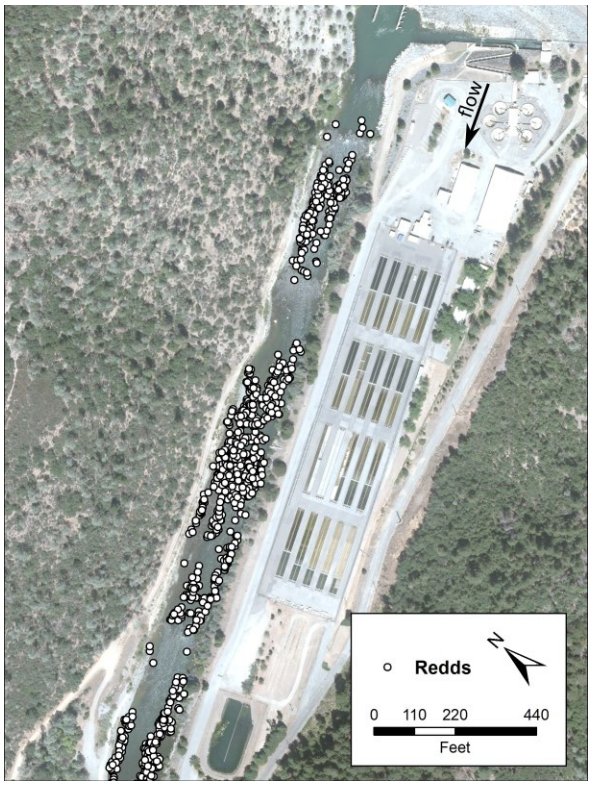

Figure 22: Redds adjacent to the Lewiston Fish Hatchery.

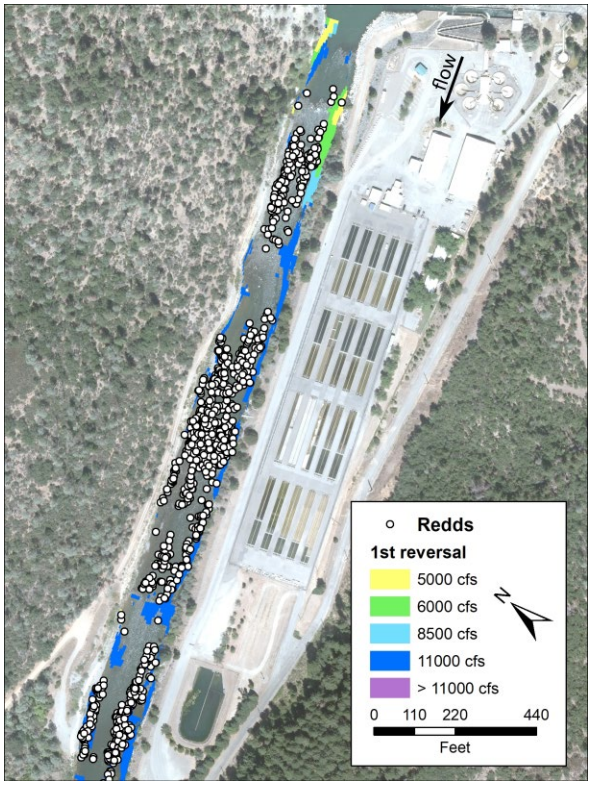

Figure 23: Map of discharges when first shear stress reversal occurs adjacent to the Lewiston Fish Hatchery.

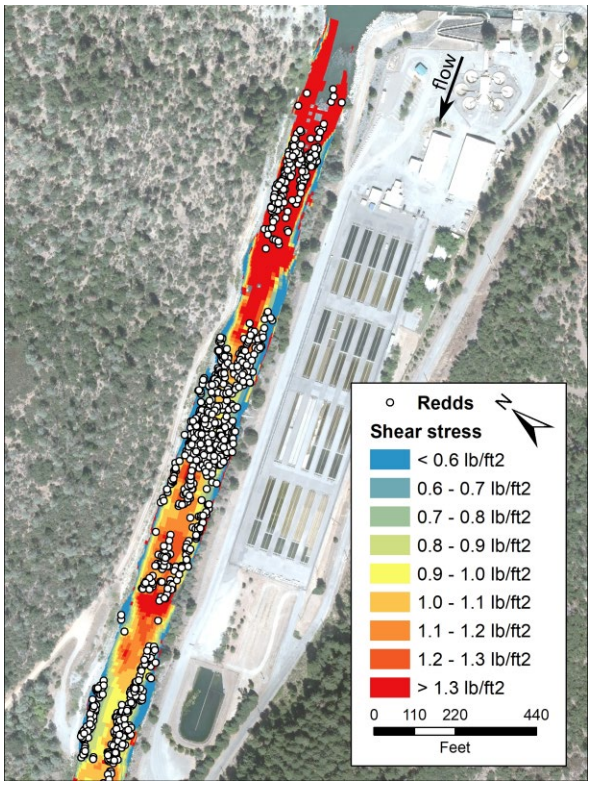

Figure 24: Map of maximum modeled shear stresses adjacent to the Lewiston Fish Hatchery.

Other explanatory variables for redd site selection

Although shear stress reversals and local hydraulics which moderate shear stress are known to be linked to bar and riffle formation, little is known about how fish discriminate between more or less favorable riffle locations for spawning. Multiple factors, including grain size and sorting, hyporheic flow, lateral inflows from groundwater or tributaries, and perhaps many more, are involved in habitat selection (Kondolf 2000; Riebe et al. 2014). Clustered breeding patterns, exhibited by salmonids, are common in the animal kingdom and many potential benefits of this strategy related to ecological, social, and genetic factors have been suggested or documented for various species (Macedo et al. 2018). The clustering of redds in areas that, according to our hydraulic model, experience shear stress reversals more frequently and at lower discharges suggests the possibility that fish can actively select for riffle stability. In other words, fish may respond to factors that convey information about the hydraulic conditions likely to exist when discharge is substantially greater than what fish experience when spawning. In fact, selecting for grain size or level of sorting is an example of the types of information that can reflect conditions at greater discharge. While clustered spawning in salmon is likely also driven by social and genetic factors, there exists the potential that a limiting ecological resource for salmonid spawning distribution is the available area which experiences moderation or reversal of shear stress over a range of flows.

Previous modeling efforts on the Trinity River to predict salmon spawning habitat quality were parameterized using variables found to be commonly associated with spawning habitat selection including distances to increase in channel slope, distance to shore, and substrate size (Goodman

et al. 2018). These variables were presented as providing either ideal conditions for hyporheic and interstitial flow through gravels or escape cover. Each of these variables may also be associated with moderated range or reversal of shear stress over a range of flows. Channel slope change is associated with riffle crests and relatively high shear stress at low flows, but these areas tend to be depositional at larger floods. Shear stress appears to be moderated or reverse more often near streambanks, attributable to roughness and eddy formation at channel margins. As previously discussed, gravels tend to accumulate in areas with shear stress too high at low flows to allow smaller sediment particles to accumulate, but sufficiently low as flows increase above thresholds of coarse sediment transport to become depositional. Whether site selection is more influenced by favorable conditions for incubation, or natural selection against individuals who spawn in areas more susceptible to scour of gametes is relatively unimportant for management, particularly because these attributes tend to co-occur. Either mechanism result in a species capable of successful reproduction in a disturbance prone environment.

Flow Management for Beneficial Bed Disturbance

The fact that shear stresses can decrease with increasing discharge in some locations means that the cumulative fractions of the stream bed subject to τ^* in excess of the bed disturbance threshold over the course of a flood hydrograph are larger than the fractions calculated for any single discharge would indicate. As $\tau^* > 0.03$ is taken here as the threshold of bed entrainment, it is assumed that the cumulative fractions of bed area that exceed that value represent the extents of ecologically beneficial bed disturbance that might be achieved by managed winter flood events (Table 5). The resulting cumulative fractions of bed disturbance exceed the fractions indicated by independent consideration of discrete discharges by less than 0.05 in most cases but tend to increase rapidly as the range of potential flood discharges in the more downstream stream segments becomes large. The maximum difference is attained for the MFF discharge in segment 7 where the cumulative fraction of bed disturbance exceeds the single-discharge fraction by 0.123.

Table 5: Cumulative fractions of the stream bed subject to $\tau^* > 0.03$ over the course of a flood hydrograph that attains the MFF in each stream segment. Cumulative fractions for the full study area are based on a flood hydrograph peaking at 11000 ft^3/s.

	Discharge, ft^3/s							
Segment	4000	5000	6000	8500	11000	16000	22000	MFF
1	0.209	0.276	0.343	0.480	0.541	na	na	0.541
2	0.194	0.247	0.295	0.399	0.436	na	na	0.448
3	0.196	0.254	0.307	0.413	0.468	na	na	0.515
4	0.249	0.308	0.372	0.497	0.551	na	na	0.619
5	0.265	0.341	0.402	0.498	0.525	0.573	na	0.584
6	0.262	0.327	0.391	0.502	0.540	0.588	na	0.614
7	0.411	0.491	0.553	0.643	0.666	0.695	0.714	0.735
All	0.261	0.328	0.388	0.496	0.536	na	na	0.587

The cumulative fraction of the bed disturbed increases at a decreasing rate as discharge increases across all stream segments and flows considered. The rate of increase in area of stream bed disturbed is between ~4-7% per 1000 ft^3/s within the discharge range from 4000 to 8500 ft^3/s. Above 8500 ft^3 the increase in disturbed area per 1000 ft^3/s drops to ~1.6% or less. These rates vary among segments, with segment 7 experiencing the highest rate of bed disturbance area for all discharges. However, the pattern of increase in cumulative fraction of the bed area disturbed across flows is consistent for all segments. It is important to note that the lowest discharge considered, 4000 ft^3/s, is predicted to disturb more than 25% of the bed, while flows of 8500 ft^3/s are predicted to disturb ~50% of the bed.

Risk of Redd Scour

As τ^* increases toward the threshold of full bed entrainment and beyond, the potential for bed scour deep enough to disturb the egg pockets buried in salmonid redds also increases. As for the general bed area, the existence of shear stress reversals also means that the fractions of redd locations that experience τ^* in excess of any particular value over a flood hydrograph is larger than the fractions calculated for single discharges. Thus, it is important to use the cumulative fractions of redd locations that exceed the relevant τ^* thresholds when assessing the potential threat to redds posed by large winter flow events.

May et al. (2009) found that $\tau^* > 0.06$ presents an estimated risk of redd scour of 8%. They suggested that risk decreases to about 3% when τ^* is between 0.04 and 0.06 and that risk falls to near zero when $\tau^* < 0.04$. As our threshold for partial mobility (0.045) is slightly greater than the value of τ^* when risk approaches zero, we conservatively assign the intermediate scour risk of 3% to that value and the higher 8% risk to $\tau^* > 0.06$, where the relevant value of τ^* at each redd location is the maximum attained at any flow up to the peak. In this way the risk of the maximum τ^* achieved at each redd over a hydrologic event achieving a given magnitude is considered, even in areas where reversals may occur. The risk of redd scour reported over the entire study area ranges from <1% at 4000 ft^3/s to slightly more than 2% at the MFF, with the highest risk occurring in segments 1 and 7 (Table 6). This level of risk is remarkably low. This is indicative of the resilience in reproduction and recovery common to disturbance adapted species. This risk should also be considered in context with other known limiting factors for production of salmonids in the Trinity River.

During the summer of 2021 spawning gravel augmentation resumed adjacent to the hatchery. High spawner abundance and density was observed in the fall and winter of 2021 after declines in spawning in the area had been observed in previous years. The gravel addition, however, did little to remedy the lack of topographic or planform structure that would provide redds with protection from scour during any high flow event that might take place during the winter. Given that some Program scientists are advocating for the inclusion of winter flow pulses in future dam operations and that Safety of Dams flow releases are sometimes required in the winter, concentrated spawning in highly mobile gravel adjacent to the hatchery could prove to be an ecological trap if flow releases achieve sufficient magnitude. Flow release magnitudes approaching 8500 ft^3/s or greater under the modeled conditions result in scour of ~2% of redds in segment 1 (Table 6). However, reduction in grain-size in the area because of augmentation would increase risk for a given flow. A more comprehensive assessment and rehabilitation plan

is needed to quantify and mitigate risk of redd scour in the hatchery reach under conditions of moderate to high dam release during incubation.

Table 6: Probability of redd scour for redds located in each stream segment for flood hydrographs peaking at discharges from 4000 ft^3/s to the local MFF discharge. Probabilities for the full study area are based on a flood hydrograph peaking at 11000 ft^3/s.

	Discharge, ft^3/s							
Segment	4000	5000	6000	8500	11000	16000	22000	MFF
1	0.0064	0.0087	0.0110	0.0187	0.0267	na	na	0.0267
2	0.0057	0.0071	0.0088	0.0122	0.0168	na	na	0.0182
3	0.0077	0.0087	0.0100	0.0119	0.0137	na	na	0.0156
4	0.0027	0.0043	0.0064	0.0106	0.0134	na	na	0.0186
5	0.0051	0.0068	0.0089	0.0128	0.0149	0.0207	na	0.0225
6	0.0045	0.0056	0.0063	0.0078	0.0091	0.0116	na	0.0144
7	0.0163	0.0187	0.0213	0.0252	0.0269	0.0296	0.0326	0.0327
All	0.0074	0.0092	0.0111	0.0159	0.0205	na	na	0.0230

Conclusions/Recommendations

Hydraulic model output predicts that τ^* increases rapidly throughout the active stream channel as discharge increases from 4000 ft^3/s to about 8500 ft^3/s. The rate of increase in τ^* then slows as discharge continues to increase beyond 8500 ft^3/s. Values of τ^* attained at 8500 ft^3/s are often close to the maxima attained at any discharge. Thus, the efficiency of flood releases for achieving ecologically beneficial bed disturbance appears to decrease for discharges greater than 8500 ft^3/s. Values of τ^* at most redd locations also tend to increase rapidly with discharge up to about 8500 ft^3/s, beyond which the rates of increase decline. An exception to this general result is found in stream segment 1, where τ^* continues to rise steeply with discharge through all potential discharges.

Redds tend to be located in areas where τ^* values span a relatively narrow range across the range of discharges. Redds tend to occupy areas with $\tau^* > 0.03$ more frequently and $\tau^* > 0.06$ less frequently than is available over the stream bed in general. Consequently, redd locations also tend to span a smaller interquartile range of τ^* values than the full stream bed. A notable exception is found with stream segment 1, for which the maximum fraction of redd locations with $\tau^* > 0.06$ exceeds the maximum fraction of the general stream bed area where that threshold is exceeded.

Although shear stresses typically increase with discharge, the locations of greatest shear can change, such that shear stresses at point locations can often decrease as discharge continues to rise. These shear stress reversals occur up to twice as frequently at redd locations than over the overall stream bed. The exception, again, is in segment 1, where reversals occur at redd locations with roughly the same frequency as they occur elsewhere.

Shear stress reversals appear to be related to changing hydraulic controls at various scales. Reversals at small to moderate flood discharges can often be traced to changes in a local hydraulic control, whereas reversals that occur at large discharges may be related to larger-scale hydraulic controls and/or the transfer of flow conveyance from the baseflow channel to overbank areas. High concentrations of salmonid redds are frequently associated with reversals that first occur at relatively small flood discharges when values of τ^* are still moderate. High concentrations of redds can also appear in areas that lack reversals, provided local rates of increase in τ^* are small so that τ^* values remain moderate at all discharges.

Shear stress reversals are conspicuously absent in the stream reach adjacent to the Trinity River Fish Hatchery where a sizable proportion of Trinity River spawners build redds. This so-called hatchery reach was artificially channelized during construction of the hatchery and lacks the geomorphic structure necessary to support complex hydraulics such as shear stress reversals. The hatchery reach is nonetheless heavily used by spawners due to its location at the end of the accessible river. This is not unexpected as the upstream end of this segment is the limit to anadromy and the location of a large federal hatchery which produces and releases salmon and steelhead. The large number of spawners using this reach accounts for the anomalous results noted above for stream segment 1, which include the hatchery reach. Given its lack of hydraulic diversity and the fact that fish will undoubtedly continue to use the reach, the hatchery reach could function under some flow release scenarios as a trap that encourages spawning while failing to provide the structure for the resulting redds to be successful. However, under modeled conditions the amount of redd scour that took place at 11000 ft^3/s, the MFF for this reach, was just over 2.5%. The gravel augmentation in the hatchery reach, which was resumed in 2021, likely increased the probability of redd scour at a given flow magnitude by decreasing the median grain-size of the bed. We recommend that TRRP develop a comprehensive restoration plan for the hatchery area that combines sediment augmentation with a civil design that establishes more of the morphologic and hydraulic complexity that presumably existed prior to channelization.

The propensity for redds to be located in areas where shear stress reversals are common could potentially be explained by noting that fish typically spawn where gravel accumulates, and such accumulations are likely to be found in areas that become depositional at higher discharges. Individual riffles vary, however, and anecdotal evidence suggests that dense clusters of redds tend to be located in areas that are prone to shear stress reversals or similar conditions that limit shear stresses to moderate magnitudes. This raises the possibility that salmonid behavior has evolved to take advantage of shear stress reversals as a means to place redds in areas that meet substrate and hyporheic flow requirements while also minimizing the risk that redds will be scoured during floods. We have no clear ideas at present about what cues might provide salmon with information about how shear stresses will change as discharge increases, but our current lack of knowledge is not sufficient grounds to dismiss the idea.

The modeling considered herein indicates that flows in the geomorphic range of management result in stream bed disturbance of areas of the stream bed from over 25% at 4000 ft^3/s to nearly 60% at the MFF. The level of disturbance accomplished by dam releases in the range of flows considered has high potential to affect BMI species composition over substantial areas of the

stream bed resulting in changes in the availability of salmonid forage in the drift and benthos. These findings highlight the importance of considering the timing and impacts of geomorphic flows on the aquatic community. Regular annual disturbance patterns have likely played an important role in the development of species phenology and life history strategies over evolutionary time. Breeding and migration time can exert strong selective pressures on a population due to the carry-over effects of resource acquisition from one life stage to the next (Harrison et al. 2011). Bed disturbance that occurs during the incubation period and prior to emergence may allow time for vulnerable prey species to proliferate in the absence of predators and competitors, while disturbance during rearing may briefly depress abundance of prey species. Migratory animals often exploit seasonal abundance to increase access to resources for offspring. Historically, the largest annual floods in the Trinity River occurred during the salmonid incubation period. Bedload sampling in the Trinity River commonly exhibits clockwise hysteresis in bedload transport rates, suggesting that early floods are most effective for mobilizing the stream bed because subsequent floods encounter a more hydraulically stable bed (Gaeuman and Stewart 2017). Prior flow management recommendations have focused on the effects of geomorphic flows on channel form and the riparian plant community, which operate and are measured on different time scales than the effects to the aquatic community described in this report.

A flow proposal developed by the TRRP during 2022 was analyzed using the modeling methods from this report. This flow proposal was developed to improve the management of environmental flow volumes and reduce the impacts of unnatural flow timing associated with storage diversion and water-forecasting (Abel 2022). The flow proposal recommends a 6500 ft^3/s Lewiston Dam release timed with significant runoff events between December 15 and February 15. A trigger of 4200 ft^3/s tributary accretion above the confluence with the North Fork Trinity River was identified as a threshold over which the release would occur. This action was applied to the hydrologic record for the period of 2004-2019. A total of six events that resulted in a flow release occurred over that time, resulting in an average increase in the area of stream bed disturbed of up to 35% in some stream segments, and potential increases in the proportion of redds at risk of scour between zero and 1.1% (Figure 25). A decreasing trend in the size of returning adult Chinook Salmon, due to earlier age at maturation, has been observed in the Klamath Basin (Shaftel 2022), as well throughout the broader range of Chinook Salmon (Oke et al. 2020). Trends in fish size and associated burial depth should be reevaluated periodically if findings are to guide future management.

While the literature has established the link between stream bed disturbance due to scouring flows and changing trophic pathways that benefit drift foraging fish (Wooton et al. 1996, Power et al. 2008, Cross et al. 2011), managers should refine approaches to achieve the ecological services provided by scouring flows by investigating impacts of varied timing, frequency, and magnitude of those events. Several studies documenting the benefits of scouring winter flows and the relative effects of natural flow timing and magnitude compared to regulated flows have been conducted in watersheds neighboring the Trinity River with very similar species assemblages and conditions (Wooton et al. 1996, Power et al. 2008). This report evaluates shear stress as a surrogate for ecological effects of flow magnitude throughout the TRRP management area and across the range of managed flows but does not address the timing and frequency of those flows. Some information regarding effects of flow timing and frequency in other streams

are available in the literature, but further investigation of those aspects of the Trinity River hydrological regime and their ecological effects could improve future efforts to provide the ecological services of stream bed disturbance.

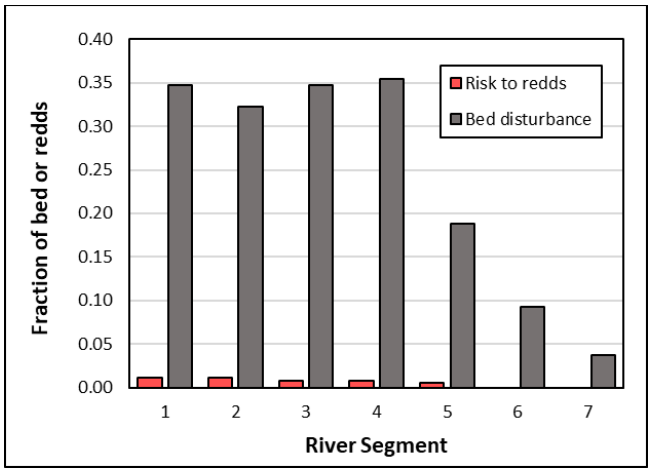

Figure 25: Increase in the fractions of stream bed disturbed and redds potentially at risk of scour due to proposed winter flow releases.

Salmon production in the Trinity River is generally considered to be limited by the juvenile freshwater life stage due to anthropogenic alteration and limited access to habitat. Several density dependent sources of mortality that result in loss of gametes or juvenile fish in freshwater exist, including pre-spawn mortality, redd superimposition, and juvenile competition. Impacts of superimposition and pre-spawn mortality likely both exceed the potential impacts from redd scour on an annual basis, even at flows as high as the MFF. The potential benefit of alleviating juvenile competition bottlenecks from limited resources, such as prey forage production or area of shear stress reversal, need to be weighed against risk of redd scour to assess the overall impact to production and inform management decisions of relative impacts in this density dependent system.

References

Abel, C.E., K.De Juilio, K.T. Lindke, S. Naman, and E.E. Thorn. 2022. *Trinity River winter flow project*. Report for the Trinity River Restoration Program, Weaverville, CA, https://www.trrp.net/library/document?id=2566.

Alvarez, J., D. Goodman, K. DeJuilio, and A. Martin, 2015. *Substrate Map. Trinity River Restoration Program Data Package*. Hoopa Tribal Fisheries, U.S. Fish and Wildlife Service, and Yurok Tribal Fisheries, Arcata, CA, https://www.trrp.net/library/data/?id=69.

Andrews, E.D., 1983. Entrainment of gravel from naturally sorted riverbed material. *Geological Society of America Bulletin* 94:1225-1231.

Andrews, E.D. and D.C. Erman. 1986. Persistence in the size distribution of surficial bed material during an extreme snowmelt flood. *Water Resources Research* 22(2):191-197.

Bjornn, T.C., and D.W. Reiser. 1991. Habitat requirements of salmonids in streams. In *Influences of Forest and Rangeland Management on Salmonid Fishes and Their Habitat*, American Fisheries Society. Spec. Pub. 19, edited by W.R. Meehan, pp. 83-138.

Bradley, D.N. 2018. *Trinity River 40 mile hydraulic model: update with 2016 Topography*. USBR Technical Services Center, Technical Report SRH-2018-11, Denver, CO, http://www.trrp.net/library/document/?id=2359.

Buffington, J.M. and D.R. Montgomery. 1997. A systematic analysis of eight decades of incipient motion studies, with special reference to gravel-bedded rivers. *Water Resources Research* 33(8):1993-2029.

Buxton, T.H., J.M. Buffington, E.M. Yager, M.A. Hassan, and A.K. Fremier. 2015. The relative stability of salmon redds and unspawned stream beds. *Water Resources Research* 51, doi:10.1002/2015WR016908.

Cao, Z., P. Carling and R. Oakey. 2003. Flow reversal over a natural pool-riffle sequence: A computational study. *Earth Surface Processes and Landforms* 28:689-705, doi: 10.1002/esp.466.

Carling, P.A. 1991. An appraisal of the velocity-reversal hypothesis for stable pool-riffle sequences in the River Severn, England. *Earth Surface Processes and Landforms* 16:19-31.

CDWR. 2007. *Trinity River hydraulic flow study: North Fork Trinity to Lewiston Dam*. California Department of Water Resources, Sacramento, CA.

Cross, W.F., C.V. Baxter, K.C. Donner, E.J. Rosi-Marshall, T.A. Kennedy, R.O. Hall, Jr., H.A. Wellard Kelly, and R.S. Rogers. 2011. Ecosystem ecology meets adaptive management: food web response to a controlled flood on the Colorado River, Glen Canyon. *Ecological Applications* 21(6):2016-2033.

DWR. 2007. *Trinity River hydraulic flow study: North Fork Trinity to Lewiston Dam*. California Department of Water Resources, Sacramento, CA

Evenson, E.F. 2001. *Egg pocket depth and particle size composition within chinook salmon redds in the Trinity River, California*. Masters thesis presented to the faculty of Humboldt State University, Arcata, CA.

FEMA. 2016. *Flood insurance study: Trinity County, California, and incorporated areas*. Federal Emergency Management Agency Flood Insurance Study No. 06105CV000C.

Ferguson, R., 2007. Flow resistance equations for gravel- and boulder-bed streams. *Water Resources Research* 43, W05427, doi:10.1029/2006WR00522.

Fetter, C.W. 1994. *Applied hydrogeology*. Prentice-Hall, Upper Saddle River, NJ, 691 pp.

Gaeuman, D. 2011. *Water year 2010 implementation monitoring report*. Trinity River Restoration Program Technical Report TR-TRRP-2011-1, Weaverville, CA, http://www.trrp.net/library/document/?id=1811.

Gaeuman, D. 2020. *WY2016-17 Trinity River gravel augmentation monitoring report.* Trinity River Restoration Program Technical Report, TR-TRRP-2020-1, Weaverville, CA, http://www.trrp.net/library/document?id=2464.

Gaeuman, D. and A. Krause. 2011. *2010 bed-material sediment budget update, Trinity River, Lewiston Dam to Douglas City, California*. Trinity River Restoration Program Technical Report TM-TRRP-2011-2, Weaverville, CA, http://www.trrp.net/library/document?id=1305.

Gaeuman, D. and R.L. Stewart. 2017. *Sediment transport in the Trinity River, CA: Data synthesis 2004-2015*. TRRP Technical Report TR-TRRP-2017-1, Trinity River Restoration Program, Weaverville, CA, http://www.trrp.net/library/document?id=2357.

Gaeuman, D. and R.L. Stewart. 2019. *WY2015 Trinity River gravel augmentation implementation monitoring report*, Trinity River Restoration Program Technical Report, TR-TRRP-2019-2, Weaverville, CA, http://www.trrp.net/library/document?id=2357.

Gaeuman, D., R. Stewart, and T. Buxton. 2016. *First steps toward a river corridor management strategy*. TRRP Technical Report TR-TRRP-2016-1, Trinity River Restoration Program, Weaverville, CA, http://www.trrp.net/library/document?id=2294.

Gaeuman, D., R.L. Stewart, B. Schmandt and C. Pryor. 2017. Geomorphic response to gravel augmentation and high-flow dam release in the Trinity River, California. *Earth Surface Processes and Landforms* 42:2523-2540, doi:10.1002/esp.4191

GMA (GMA Hydrology). 2017. *2016 Trinity River focal reach survey report*. Report to the Trinity River Restoration Program, Weaverville, CA, http://www.trrp.net/library/document?id=2389.

Goodman, D.H., N.A. Som, and N.J. Hetrick. 2018. Increasing the availability and spatial variation of spawning habitats through ascending baseflows. *River Research and Applications* 34:844-853. DOI: 10.1002/rra.3302.

Harrison, X.A., J.D. Blount, R. Inger, D.R. Norris, and S. Bearhop. 2011. Carry-over effects as drivers of fitness differences in animals. *Journal of Animal Ecology* 80:4-18.

Keller, E.A. 1971. Areal sorting of bed-load material: the hypothesis of velocity reversal. *Geological Society of America Bulletin* 82(3):753-756.

Kondolf, G.M. 2000. Assessing salmonid spawning gravel quality. *Transactions of the American Fisheries Society* 129:262-281.

Lai, Y.G. 2010. Two-dimensional depth-averaged flow modeling with an unstructured hybrid mesh. *Journal of Hydraulic Engineering* 136(1):12-23.

Lisle, T. E. 1979. A sorting mechanism for a riffle-pool sequence. *Geological Society of America Bulletin* 90, 616–617.

Lisle, T.E., J.M. Nelson, J. Pitlick, M.A. Madej and B.L. Barkett. 2000. Variability of bed mobility in natural, gravel-bed channels and adjustments to sediment load at local and reach scales. *Water Resources Research* 36(12):3743-3755.

May, C.L., B. Pryor, T.E. Lisle, and M. Lang. 2009. Coupling hydrodynamic modeling and empirical measures of bed mobility to predict the risk of scour and fill of salmon redds in a large regulated river. *Water Resources Research* Vol. 45, W05402, doi:10.1029/2007WR006498.

MacWilliams, M.L. Jr., J.M. Wheaton, G.B. Pasternak, R.L. Street and P.K. Kitanidis. 2006. Flow convergence routing hypothesis for pool-riffle maintenance in alluvial rivers. *Water Resources Research* Vol. 42, W10427, doi:10.1029/2005WR004391.

Macedo, R.H., J. Podos, J.A. Graves, and L.T. Manica. 2018. Breeding clusters in birds: ecological selective contexts, mating systems and the role of extrapair fertilizations. *Animal Behavior,* http://doi.org/10.1016/j.anbehav.2018.01.021

Montgomery, D.R., J.M. Buffington, N.P. Peterson D. Schuett-Hames, and T.P. Quinn. 1996. Stream-bed scour, egg burial depths, and the influence of salmonid spawning on bed surface mobility and embryo survival. *Canadian Journal of Fisheries and Aquatic Sciences* 53:1061-1070.

Murry, C.B. and J.D. McPhail. 1987. Effect of incubation temperature on the development of five species of Pacific salmon (Oncorhynchus) embryos and alevins. *Canadian Journal of Zoology* 66:266- 213.

Oke, K.B., C.J. Cunningham, P.A.H. Westley, M.L. Baskett, S.M. Carlson, J. Clark, A.P. Hendry, V.A. Karatayev , N.W. Kendall, J. Kibele , H.K. Kindsvater, K.M. Kobayashi1 , B. Lewis, S. Munch, J.D. Reynolds, G.K. Vick, and E.P. Palkovacs. 2020. Recent declines in salmon body size impact ecosystems and fisheries. *Nature Communications* 11:4155, doi.org/10.1038/s41467-020-17726-z

Parker, G. 1990. Surface-based bedload transport relation for gravel rivers. *Journal of Hydraulic Research* 28:417-436.

Pasternack, G.B, M.K. Bounrisavong, and K.K. Parikh. 2008. Backwater control on riffle–pool hydraulics, fish habitat quality, and sediment transport regime in gravel-bed rivers. *Journal of Hydrology* 357:125– 139, doi:10.1016/j.jhydrol.2008.05.014.

Power, M.E., M.S. Parker, and W.E. Dietrich. 2008. Seasonal Reassembly of a River Food Web: Floods, Droughts, and Impacts of Fish. *Ecological Monographs* 78(2):263-282.

Riebe, C.S., L.S. Sklar, B.T. Overstreet, and J.K. Wooster. 2014. Optimal reproduction in salmon spawning substrates linked to grain size and fish length. *Water Resources Research* 50, doi:10.1002/2013WR014231.

Ritter, J.R. 1968. *Changes in the channel morphology of Trinity River and eight tributaries, California, 1961-65*. US Geological Survey Open-File Report, Menlo Park, CA.

Rupert, D.L., C.D. Chamberlain, S.A. Gough, N.A. Som, N.J. Davids, W.C. Matilton, A.M. Hill, and E.R. Wiseman. 2017. *Mainstem Trinity River Chinook Salmon Spawning Distribution*

2012–2014. U.S. Fish and Wildlife Service. Arcata Fish and Wildlife Office, Arcata Fisheries Data Series Report Number DS 2017–52, Arcata, CA.

Shaftel, D.D. 2022. *Managing Uncertainty: Forecasting Ocean Abundance of Klamath River Fall-Run Chinook Salmon (Oncorhynchus tshawytscha)*. Masters thesis presented to the faculty of Scripps Institution of Oceanography, UC San Diego, CA.

Sparkman, M.D. 2003. *Negative influences of predacious egg-eating worms, Haplotaxis ichthyophagous, and fine sediment on coho salmon, Oncohynchus kisutch, in natural and artificial redds.* Masters thesis presented to the faculty of Humboldt State University, Arcata, CA.

Tonina, D., and Buffington, J.M. 2009. A three-dimensional model for analyzing the effects of salmon redds on hyporheic exchange and egg pocket habitat. *Canadian Journal of Fisheries and Aquatic Sciences* 66: doi:10.1139/F09-146.

USDOI (United States Department of the Interior). 2000. *Record of Decision: Trinity River mainstem fishery restoration final environmental impact statement/environmental impact report*. Washington D.C.

USGS (US Geological Survey). 1981. *Guidelines for determining flood flow frequency*. US Water Resources Council Bulletin 17B, US Government Printing Office, Washington, D.C.

Wilcock, P.R. and B.W. McArdell. 1993. Surface-based fractional transport rates: mobilization thresholds and partial transport of a sand-gravel sediment. *Water Resources Research* 29(4):1297-1312.

Wilkinson, S. N., Keller, R. J., and Rutherfurd, I. D. 2004. Phase-shifts in shear stress as an explanation for the maintenance of pool-riffle sequences. *Earth Surface Processes and Landforms* 29:737–753.

Wolman, M.G. 1954. A method of sampling coarse river-bed materials. *Transactions, American Geophysical Union* 35(6):951-956.

Wootton, J. T., M.S. Parker, and M.E. Power. 1996. Effects of disturbance on river food webs. *Science* 273(5281):1558–1561, http://www.jstor.org/stable/2891058.

Yurok Tribe and NHE (Northern Hydrology and Engineering). 2017. *Final design report: Trinity River Program Sheridan Creek channel rehabilitation project*. Report to the Trinity River Restoration Program, Weaverville CA.

Appendix A: Substrate Particles Size Transformation

Multiple methods for sampling granular Earth materials exist, and the appropriate method to use in a given situation depends on the nature of the question being investigated. Following the comprehensive review of sediment sampling provided by Bunte and Abt (2001), we distinguish three basic ways to sample unconsolidated sediments: volumetric sampling, grid-based sampling in which samples are collected from pre-established points on a grid or transect, and areal samples in which all particles within a pre-defined area are collected. Each of these three types of samples can be quantified in terms of the number of particles within each particle size class or by the weight of the material within each size class, leading to the potential for six distinct sample metrics. For studies of sediment mobility and most other geomorphic assessments, stream bed sediments are typically described in terms of volume-by-weight (bulk samples) or in terms of grid-by-number (pebble count). The remaining four possibilities (volume-by-number, area-by-number, grid-by-weight, and area-by- weight) are rarely used in the context of fluvial sediment mobility. Of these remaining four, area-by-number sampling, in which the number of particles in each size class within a pre-defined sampling area, is of special significance in the discussion to follow.

The different sampling procedures outlined above generally result in different particle size distributions that yield different sizes for a given particle percentile. These differences can be illustrated with a voidless cube model introduced by Kellerhals and Bray (1971) and described in detail by Bunte and Abt (2001). This cube model represents a mixture of cubic particles of three sizes packed together with no void space. A third of the total volume of the model is taken up by cubes with a diameter (D) of length 1 (the units of length are immaterial). Another third of the total volume is taken up by cubes with $D = 2$, and the remaining third is filled with cubes with $D = 4$ (Figure A-1). Assuming the cubes are packed randomly, each size class will also take up an equal area (1/3 of the total) of the surface of the cube model. The number of cubes of each size that appear on the model surface, however, is not equal. Instead, 16 times more of the smallest cubes ($D = 1$) will appear on the surface than of the largest cubes ($D = 4$), and the number of the smallest cubes on the surface will be 4 times greater than the number of intermediate sized cubes ($D = 2$).

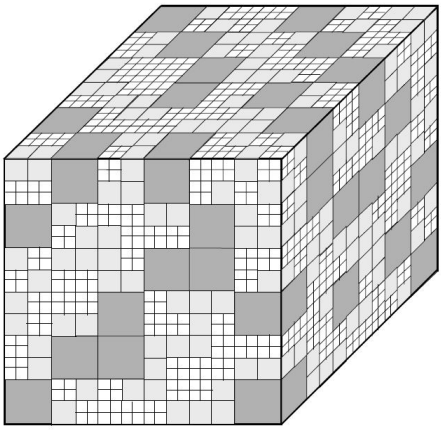

Figure A-1: Illustration of the voidless cube model as presented by Bunte and Abt (2001).

Due to the relatively small number of large cubes that appear on the model surface, an area-by-number sample in which all cubic particles within a given area are collected would result in a sample size distribution with a large fraction of particles of $D = 1$ and very small fraction with $D = 4$. A grid-by-number sample, however, would tend to include a far larger fraction of particles with $D = 4$ in the sample because the sample points in the pre-established grid would be more likely to fall on large particles with large surface area. The grid-based sample will therefore result in larger particle size percentile values than those derived from an area-based sample. In the case of the cube model described here, the D_{84} determined from a grid-by-number sample is about 3 units, whereas the D_{84} determined from an area-by-number sample is only about 1.4 units (red curves in Figure A-2). It is also worth noting that the two types of sampling commonly applied to geomorphic studies – grid-by-number and volume-by-weight – yield identical particle size distributions.

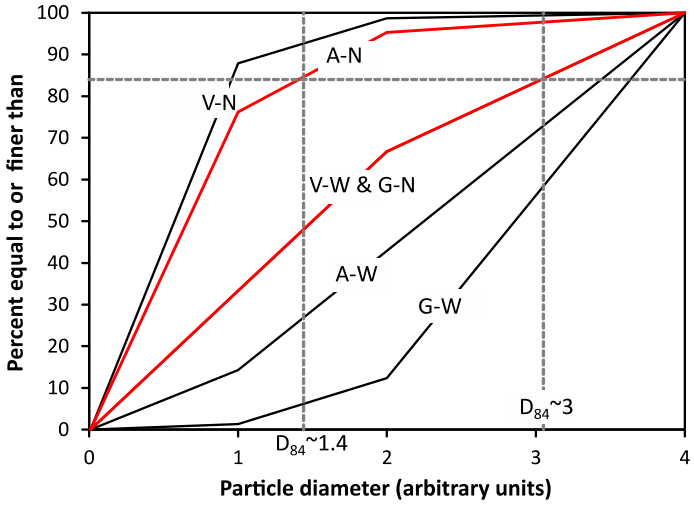

Figure A-2: Grain size distributions derived from the voidless cube model using grid-by-number (G-N), area-by-number (A-N), volume-by-number (V-N), volume-by- weight (V-W), area-by- weight (A-W), and grid-by- weight (G-W) sampling methods. Redrawn from Bunte and Abt (2001).

Returning now to the 2014 substrate map that provides the basis for our assessment of bed mobility, conversations with several members of the field crew that conducted the mapping indicated that their understanding of a "pebble count" at the time of the field work was consistent with randomly selecting 100 particles and then choosing the 84th largest stone as the D_{84}. This sampling method is akin to area-by-number sampling or perhaps to a hybrid between area-by-number sampling and the grid-by-number method conventionally used in geomorphology. This difference in sampling protocol likely explains why the 2014 map typically indicates D_{84} values that are noticeably smaller than earlier mapping efforts would suggest.

For this study, we correct for this misconception about what a pebble count sample represents and simultaneously convert the D_{84} estimates from the 2014 map (hereafter denoted $D_{84(2014)}$) to D_{50} with a transformation developed by comparing the 2014 map with substrate maps from 2006-2009 and maps presented in May et al. (2009). The 2006-2009 maps available for this

comparison consists of polygons depicting stream bed areas with similar surface textures. Commonly referred to as sedimentary facies, these areas were assigned ocular estimates of D_{50}, D_{90}, and the fraction of sand on the bed surface. The boundaries of the polygons, which were sketched on aerial photographs in the field, are approximate. In addition, some areas that were difficult to see due to high flow velocities or especially deep water were left unmapped.

The available substrate maps include one drawn in 2006 that spans RM 83.45 to 80.5 along Sky Ranch road, another from near Lewiston Dam (RM 111.8) to Weaver Creek (RM 94) compiled from data obtained in 2006 and 2007, a 2008 re-mapping of the Indian Creek project reach upstream from Weaver Creek (RM 96.8 to 94), and a 2009 mapping the Upper Junction City project reach (RM 80.5 to 79.8) that extended the Sky Ranch map to the Dutch Creek bridge in Junction City. Much of the area covered by the 2006 through 2009 maps was deemed unsuitable for comparing with the 2014 maps due to the changes that had occurred in the river between those years. Numerous rehabilitation projects and gravel augmentations completed in the Lewiston and Douglas City area, as well as at Upper Junction City, disqualified those areas. In addition, substantial natural changes disqualified other areas, such as the reaches at and downstream from the Rush Creek delta. In the end, comparisons between the 2014 and older maps were confined to the Poker Bar canyon section (RM 104 to 97.1), the reach along Sky Ranch Road where no rehabilitation projects had been implemented as of 2014, and to the Indian Creek and Upper Junction City reaches, both of which were mapped after rehabilitation projects were completed.

Having selected map reaches for comparison with $D_{84(2014)}$, we assessed the general quality of the older maps through a comparison with an intensive mapping effort from the geomorphic literature. May et al. (2009) mapped substrate in the Sheridan Creek reach, located along Sky Ranch Road at RM 82.2 to 81.45, in 2005 as part of a 3-year study to evaluate the potential for winter floods to scour salmon redds in the area. They employed grid-by-number sampling of the stream bed surface, using snorkel or even scuba gear as necessary, to obtain surface particle-size distributions at 93 locations throughout the reach. Particle-size metrics including the D_{50} were computed for each location and interpolated to particle size maps. Their paper presents a figure showing the map corresponding to the D_{50} with grain sizes classified into grain-size bins (Figure A-3). We digitized that map, converted it to a 2-ft grid, and used a spatial join in ArcMap to match those grain-size bins to D_{50} values we mapped in 2006. When displayed side-by-side with the same color ramp, the two maps are visually similar (Figure A-3), and point-by-point analyses indicate that 62% of the D_{50} values interpolated from the 2006 facies map match the size classes given by the May et al. (2009) map. We therefore concluded that the selected D_{50} maps from the 2006-2009 mapping efforts are suitable for converting $D_{84(2014)}$ to grid-by-number D_{50} values.

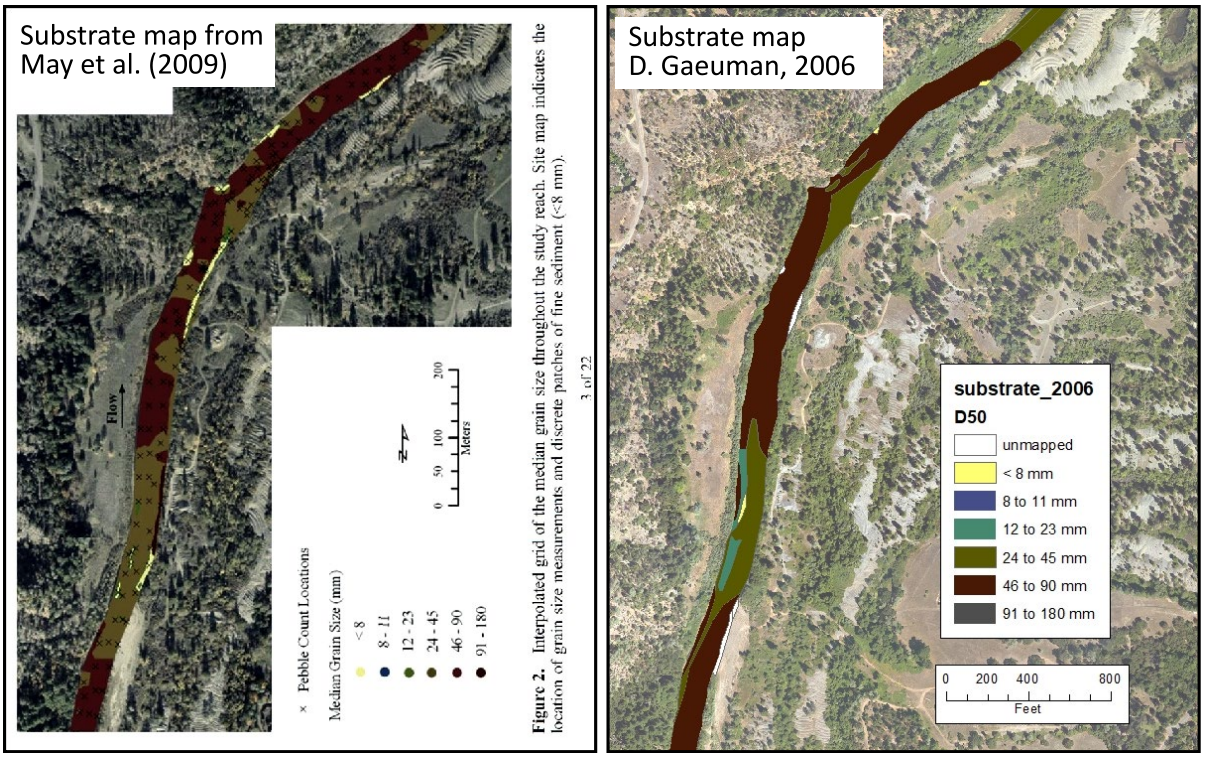

Figure A-3: Binned D_{50} particle sizes presented by May et al. (2009) compared with binned D_{50} values mapped in 2006.

The first step in the development of that conversion was to match point values of $D_{84(2014)}$ to point values of D_{50} interpolated from the older maps via spatial join. We then applied ordinary least squares regression to a plot of D_{50} versus $D_{50}/D_{84(2014)}$ to obtain a best-fit line with R^2 = 0.44, and algebraically manipulated the regression equation to obtain:

$$D_{50} = 0.284/[1/D_{84(2014)} - 0.0054] \qquad (2)$$

Equation (2) casts the derived value of D_{50} as a nonlinear function of $D_{84(2014)}$ because the bias associated with the sampling scheme used for the 2014 mapping effort depends on the estimated $D_{84(2014)}$ particle size and the shape of the particle size distribution. Consider a patch of substrate composed of 100 particles that range in size from 1 mm to 100 mm, where particle number n is n mm in diameter. This represents an unrealistically smooth and uniform distribution that is described here only for the sake of simplicity. If one were to choose the 16th largest particle from one of the 100 particle sets to represent the D_{84}, which is analogous to what was done during the $D_{84(2014)}$ data collection effort, that percentile would be estimated at 85 mm in diameter. Similarly, if the 50th largest particle was chosen to represent the D_{50}, that percentile would be estimated at 50 mm. If, however, one were to randomly sample the same patch of substrate 100 times using a grid-based method, the fact that the area occupied by each particle scales as the square of its diameter would mean that each random sample points would land on larger particles more frequently. The resulting D_{84} determined from such a sample would most likely be near 94 mm and the D_{50} would be near 80 mm. Thus, the estimate of D_{84} determined as the 16th largest particle in a set of 100 particles would be considerably smaller than the D_{84} determined from a

grid-by-number sample. In this example, the incorrect D_{84} is actually closer in size to the correctly sampled D_{50} than to the correctly sampled D_{84}.

Now consider a similar population of particles in which the larger particles are very large compared to the smaller particles. An example would be a population composed of many sets of 100 particles in which particle number n is n mm in diameter for particles 1 through 75 but each of particles 76 through 100 are 3 mm larger than the preceding particle. The 16th largest particle would now be 125 mm in diameter, whereas the true D_{50} determined with a grid-by-number sample from the same probability distribution would be about 145 mm. That is, the incorrectly sampled D_{84} can actually be smaller than the correctly sampled D_{50} in some situations.

These two simple examples should make it clear that converting $D_{84(2014)}$ values to D_{50} values cannot be accomplished with a constant conversion factor. The first example shows that, as the particle size distribution becomes more uniform, the ratio of the actual D_{50} to the estimated $D_{84(2014)}$ will tend to increase toward unity and eventually converge at that value. This makes intuitive sense if one considers that, in the limit, any estimate of D_{84} that approaches the size range of sand implies that the substrate has transitioned from a gravel bed to a sand bed and distinguishing between D_{84} and D_{50} is no longer possible with pebble counting techniques. Plotting $D_{50}/D_{84(2014)}$ as a function of $D_{84(2014)}$ according to equation (2) reveals that $D_{50}/D_{84(2014)}$ decreases with decreasing $D_{84(2014)}$ and ultimately fall below 0.3 as $D_{84(2014)}$ approaches zero. Equation (2), therefore, cannot apply to substrates for which the estimated $D_{84(2014)}$ is small. We therefore defined a second relationship relating D_{50} to $D_{50}/D_{84(2014)}$ by linearly interpolating between the value of $D_{50}/D_{84(2014)}$ obtained for 50 mm from equation (2) and $D_{50}/D_{84(2014)} = 1$ when $D_{84(2014)} = 1$ mm. Rearranging that equation to solve for D_{50} yields:

$$D_{50} = 1.036/[1/D_{84(2014)} + 0.0327], \quad D_{84(2014)} < 50 \text{ mm} \qquad (3)$$

The second of the two examples described above shows that, as the particle size distribution become broader, estimates of $D_{84(2014)}$ will be biased toward larger particles and $D_{50}/D_{84(2014)}$ will tend to increase without bound. Equation (2) will produce $D_{50}/D_{84(2014)} > 1$ for large $D_{84(2014)}$, which may be correct in some instances, but the magnitude of the increase becomes unreasonably large if that equation is continued much past the small cobble range (> 128 mm). What constitutes a realistic value of $D_{50}/D_{84(2014)}$ for the largest estimates of $D_{84(2014)}$ cannot be determined at this point, because that depends on how individual members of the field crew that mapped the substrate interpreted areas of substrate that include very large particles. We suspect that the field personnel would resist choosing a relatively small particle as D_{84} when confronted by a boulder-dominated substrate, so we assume that their D_{84} estimates for those substrates are not substantially smaller than the true D_{50}. We therefore adopted an upper limit of 1.2 for $D_{50}/D_{84(2014)}$, which is attained by equation (2) at $D_{84(2014)} = 140$ mm. Thus, the set of equations needed to transform $D_{84(2014)}$ to D_{50} is completed with:

$$D_{50} = 1.2\, D_{84(2014)}, \quad D_{84(2014)} > 140 \text{ mm} \qquad (4)$$

Despite the somewhat arbitrary nature of the upper limit on $D_{50}/D_{84(2014)}$ imposed by equation (4), we do not believe uncertainty in transforming the largest $D_{84(2014)}$ values to D_{50} represents a major problem for our analyses. Regions of very coarse substrate are not normally locations

where salmonid redds are found, so the results of the transformation in those areas is of little consequence for our investigation into the relationship between τ^* and the locations of redds. Likewise, areas of substrate composed of large cobbles and boulders can be expected to experience relatively low τ^* across the full range of relevant discharges, so accurately determining τ^* in those areas is not critical for assessing the spatial distribution of bed disturbance.

Figure A-4 depicts the behavior equations (2-4), as applied to their appropriate ranges of $D_{84(2014)}$. In summary, the ratios of the computed D_{50} values to the $D_{84(2014)}$ values are smallest for $D_{84(2014)}$ near 50 mm. Values of $D_{50}/D_{84(2014)}$ rapidly increase to near unity as $D_{84(2014)}$ approaches 8 mm at the small end of the particle size range and increase more slowly as $D_{84(2014)}$ increases toward the coarse end of its range. $D_{50}/D_{84(2014)}$ reaches a maximum of 1.2 when $D_{84(2014)}$ reaches 140 mm.

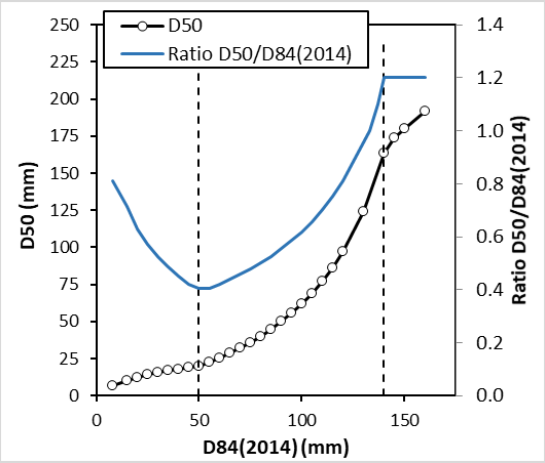

Figure A-4: Relationship between transformed D_{50} and $D_{84(2014)}$ with $D_{50}/D_{84(2014)}$ shown in blue. Dashed vertical line indicated boundaries between the domains of the three transformation equations.

We assessed the performance of equations (2-4) by comparing calculated values of D_{50} with D_{50} values drawn from the 2006 substrate maps. We computed root mean square (RMS) errors for three size ranges of particles: The fine end of the particle size distribution is represented by $20 \leq D_{50} < 32$ mm and the coarse end is represented by $128 < D_{50} \leq 256$ mm. The remaining portion of the distribution ($32 \leq D_{50} \leq 128$ mm) constitutes 74% of the mapped bed area and is considered the most suitable substrate size range for salmonid spawning. For that intermediate size range, the RMS difference between the derived D_{50} values and those mapped in 2006 is 0.6 ϕ, where ϕ is the base-2 logarithm of particle size (Fetter 1994). When converted to mm, that RMS error is equivalent to about 42% of the particle size. The mean RMS error for the intermediate size range is 0.03 ϕ, which for a particle in the middle of that size range corresponds to a mean error of less than 2 mm. RMS errors for the fine and coarse tails of the full particle size distribution are larger than those found for intermediate particle sizes. At 0.94 ϕ for the fine tail and 1.1 ϕ for the coarse tail, the errors are equivalent to a factor of about 2. Accuracy at the tails

of the distribution, however, are not considered critical to our analyses because the behavior of especially coarse and fine portions of the bed are not central to the issues being investigated.

We consider the level of uncertainty obtained for the central part of the particle size distribution to be satisfactory given the number and magnitude of the potential errors in the available data. Major sources of uncertainty include inaccuracies and inconsistencies in the ocular estimates of D_{84} obtained in 2014, interpolation errors associated with creation of the $D_{84(2014)}$ maps, inaccuracies in the ocular estimates of D_{50} mapped in 2006, the relatively coarse spatial resolution of the 2006 maps, and potential changes in substrate conditions during the 8 years that separate the two mapping efforts. Given these challenges, it is somewhat surprising that the transformation performs as well as it does. It should nonetheless be understood that individual estimates of D_{50}, and therefore individual values of τ^*, should not be regarded as being accurate regardless of particle size. The derived D_{50} and τ^* values are meaningful only in a statistical sense. That is, they are taken to approximate substrate and hydraulic conditions present in the river during the 2012-2016 time frame only when aggregated as statistical quantities based on large samples that span large regions of stream bed.

References

Bunte, K. and S.R. Apt, 2001. *Sampling surface and subsurface particle-size distribution in wadable gravel- and cobble-bed streams for analyses in sediment transport, hydraulics, and stream bed monitoring*. Rocky Mountain Research Station General Technical Report RMRS-GTR-74, USDA Forest Service.

Fetter, C.W. 1994. *Applied hydrogeology*. Prentice-Hall, Upper Saddle River, NJ, 691 pp.

Kellerhals, R. and D.I. Bray, 1971. Sampling procedures for coarse fluvial sediments. *Journal of the Hydraulics Division*, ASCE 97 (HY8):1165-1180.

May, C.L., B. Pryor, T.E. Lisle, and M. Lang, 2009. Coupling hydrodynamic modeling and empirical measures of bed mobility to predict the risk of scour and fill of salmon redds in a large regulated river. *Water Resources Research* Vol. 45, W05402, doi:10.1029/2007WR006498.